Voltage-Gated Na^+ Channels

- Voltage-Gated Na^+ Channels Introduction
- Voltage-Gated Na^+ Channel Regulation, Nomenclature and Channelopathies
- References

Click Channel Type to Access Validation Data:

$Na_V1.1$
$Na_V1.2$
$Na_V1.3$
$Na_V1.4$
$Na_V1.5$
$Na_V1.6$
$Na_V1.7$
$Na_V1.8\beta_1$
r$Na_V1.8$ (ND7-23 Cells)

Please press the "Back" button to return to the previous menu

BACK

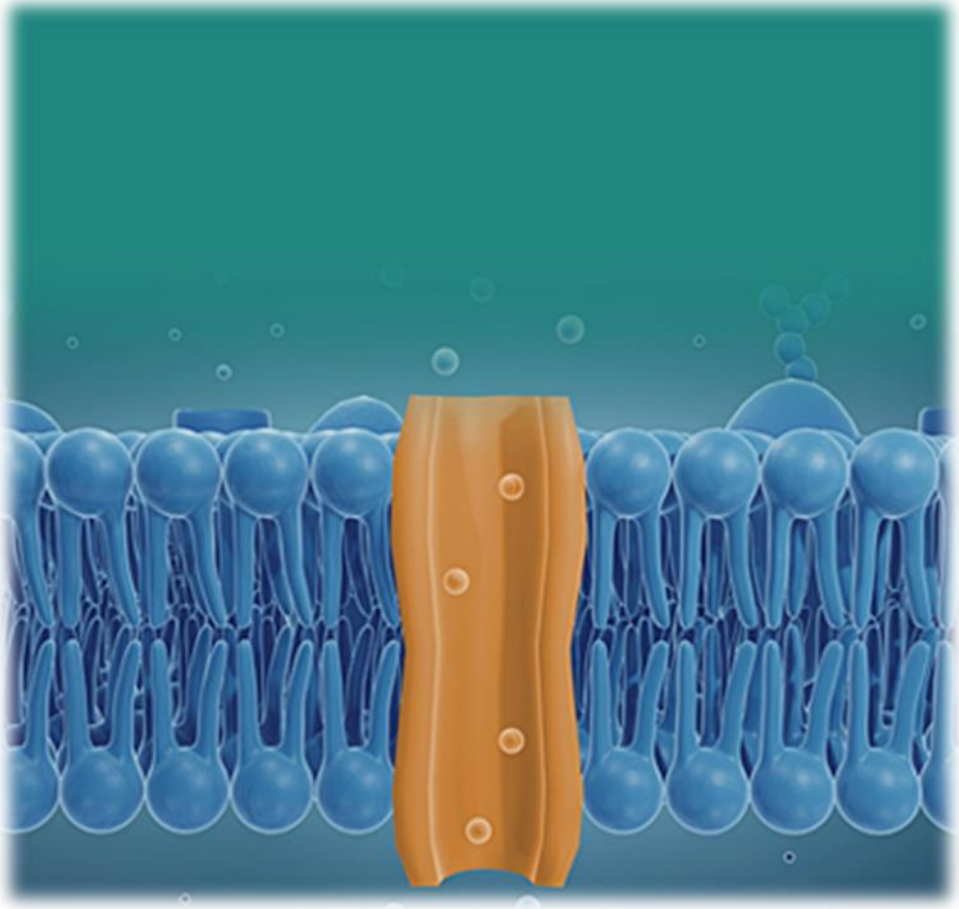

Voltage-Gated Na^+ Channels Introduction

BACK

In excitable cells voltage-gated sodium channels are responsible for action potential initiation and propagation. These include nerve, muscle, and neuroendocrine cells [1,2]. Nonexcitable cells also express voltage-gated sodium channels where their role is less clear [3]. Sodium channels were the first ion channel protein where the sequence of amino acids was deduced from cDNA [4]. This was done in a purified preparation from eel electric organs originally identified as the tetrodotoxin binding component in the eel [5].

Sodium channels consist of a large (~260 kD) pore forming α subunit, associated with auxiliary β subunits ranging from approximately 30-40 kDa [6]. Central nervous system (CNS) and cardiac sodium channels contain a mixture of β subunits (β1 - β4), skeletal muscle sodium channels only have the β1 subunit [7,8]. The pore-forming α subunit alone does function as a sodium channel, but voltage-dependent gating and ionic current kinetics are affected by β subunits. Channel localization, interaction with cell adhesion molecules, the extracellular matrix and intracellular cytoskeleton are also affected by the β subunits. The α subunits consists of four homologous domains (I–IV), each of which consist of six transmembrane alpha helices (S1–S6). The pore itself is located in a loop between the S5 and S6 segments [6]. The voltage sensor consists of charged amino acid residues in the S4 segments of each domain. These can be measured as gating currents and function by moving across the membrane response to depolarization resulting in channel activation. Inactivation of the channel is achieved by a short intracellular loop connecting domains III and IV, it folds into the channel structure physically blocking the pore during sustained membrane depolarization

Voltage-Gated Na^+ Channel Regulation, Nomenclature and Channelopathies

Sodium channels are regulated by proteins including protein kinases and G proteins that transiently interact with them [9]. Other proteins including cell adhesion molecules and cytoskeletal proteins interact more permanently and are involved in subcellular targeting and localization [9].

A standardized nomenclature has been developed for voltage-gated sodium channels [27]. This nomenclature is based on that for voltage-gated potassium channels [10]. Subfamilies and sub-types are defined based on similarities between the channels amino acid sequence. The name of an individual channel consists of permeating ion (Na) with voltage indicated as a subscript (Na_V). The gene subfamily then follows, since only one Na_V subfamily has been identified that nomenclature is Na_V1, followed by a decimal point and the specific channel isoform (e.g. $Na_V1.5$), in the approximate order in which each sodium channel gene was identified.

Many genetic diseases are caused by mutations of sodium channels, including inherited forms of epilepsy, cardiac arrhythmia, migraine, periodic paralysis, peripheral neuropathy, and chronic pain [11-19]. In most cases, the mutations that cause these diseases are caused by a gain-of-function effect on the sodium channels leading to cellular hyperexcitibility. Exceptions to this are Dravet Syndrome where NaV1.1 has a loss of function leading to a reduction in action potential firing in GABAergic inhibitory interneurons leading to childhood epilepsy syndrome [20] Another exception is Congenital Indifference to Pain, where loss-of-function mutations in the gene encoding NaV1.7 channels cause complete loss of pain sensation and great risk of injury to the patient due to lack of pain feedback from their surroundings [21].

References

1. Hille B. (2001) Ionic Channels of Excitable Membranes, 3rd Ed. In (Sinauer Associates Inc.)

2. Hodgin AL, Huxley AF. (1952) A quantitative description of membrane current and its application to conduction and excitation in nerve. J Physiol (Lond.), 117 (4): 500-44. [PMID:12991237]

3. Black JA, Waxman SG. (2013) Noncanonical roles of voltage-gated sodium channels. Neuron, 80 (2): 280-91. [PMID:24139034]

4. M. Noda, S. Shimizu, T. Tanabe, T. Takai, T. Kayano, T. Ikeda, H. Takahashi, H. Nakayama, Y. Kanaoka, N. Minamino, K. Kangawa, H. Matsuo, M. Raftery, T. Hirose, S. Inayama, H. Hayashida, T. Miyata, S. Numa, Primary structure of Electrophorus electricus sodium channel deduced from cDNA sequence. Nature 312, 121-127 (1984).

5. Agnew, WS, Levinson, SR, Brabson, JS, Raferty, MA (1978) Purification of the tetrodotoxin-binding component associated with the voltage-sensitive sodium channel from Electrophorus electricus electroplax membranes. Proc Natl Acad Sci U S A. 1978 Jun; 75(6): 2606–2610 [PMID: 275831]

6. Catterall WA. (2000) From ionic currents to molecular mechanisms: the structure and function of voltage-gated sodium channels. Neuron, 26 (1): 13-25. [PMID:10798388]

7. Brackenbury WJ, Isom LL. (2011) Na Channel β Subunits: Overachievers of the Ion Channel Family. Front Pharmacol, 2: 53. [PMID:22007171]

8. Isom LL. (2001) Sodium channel beta subunits: anything but auxiliary. Neuroscientist, 7 (1): 42-54. [PMID:11486343]

9. Catterall WA. (2010) Signaling complexes of voltage-gated sodium and calcium channels. Neurosci Lett, 486 (2): 107-16. [PMID:20816922]

10) Chandy KG, Gutman GA. (1993) Nomenclature for mammalian potassium channel genes. Trends Pharmacol Sci, 14 (12): 434. [PMID:8122319]

11) Catterall WA, Dib-Hajj S, Meisler MH, Pietrobon D. (2008) Inherited neuronal ion channelopathies: new windows on complex neurological diseases. J Neurosci, 28 (46): 11768-77. [PMID:19005038]

12) Clancy CE, Kass RS. (2002) Defective cardiac ion channels: from mutations to clinical syndromes. J Clin Invest, 110 (8): 1075-7. [PMID:12393842]

BACK

References

BACK

13) Dib-Hajj SD, Yang Y, Black JA, Waxman SG. (2013) The Na(V)1.7 sodium channel: from molecule to man. Nat Rev Neurosci, 14 (1): 49-62. [PMID:23232607]

14) Escayg A, Goldin AL. (2010) Sodium channel SCN1A and epilepsy: mutations and mechanisms. Epilepsia, 51 (9): 1650-8. [PMID:20831750]

15) Faber CG, Hoeijmakers JG, Ahn HS, Cheng X, Han C, Choi JS, Estacion M, Lauria G, Vanhoutte EK, Gerrits MM et al.. (2012) Gain of function Nav1.7 mutations in idiopathic small fiber neuropathy. Ann Neurol, 71 (1): 26-39. [PMID:21698661]

16) George AL. (2005) Inherited disorders of voltage-gated sodium channels. J Clin Invest, 115 (8): 1990-9. [PMID:16075039]

17) Keating MT, Sanguinetti MC. (2001) Molecular and cellular mechanisms of cardiac arrhythmias. Cell, 104 (4): 569-80. [PMID:11239413]

18) Lehmann-Horn F, Jurkat-Rott K. (1999) Voltage-gated ion channels and hereditary disease. Physiol Rev, 79 (4): 1317-72. [PMID:10508236]

19) Venance SL, Cannon SC, Fialho D, Fontaine B, Hanna MG, Ptacek LJ, Tristani-Firouzi M, Tawil R, Griggs RC, CINCH investigators. (2006) The primary periodic paralyses: diagnosis, pathogenesis and treatment. Brain, 129 (Pt 1): 8-17. [PMID:16195244]

20) Catterall WA. (2014) Sodium channels, inherited epilepsy, and antiepileptic drugs. Annu Rev Pharmacol Toxicol, 54: 317-38. [PMID:24392695]

21) Cox JJ, Reimann F, Nicholas AK, Thornton G, Roberts E, Springell K, Karbani G, Jafri H, Mannan J, Raashid Y et al.. (2006) An SCN9A channelopathy causes congenital inability to experience pain. Nature, 444 (7121): 894-8. [PMID:17167479]

22) Catterall WA, Goldin AL, Waxman SG. Voltage-gated sodium channels (NaV) (version 2019.3) in the IUPHAR/BPS Guide to Pharmacology Database. IUPHAR/BPS Guide to Pharmacology CITE. 2019; 2019(3). Available from: https://doi.org/10.2218/gtopdb/F82/2021.3.

$Na_V1.1$ (CYL3009)

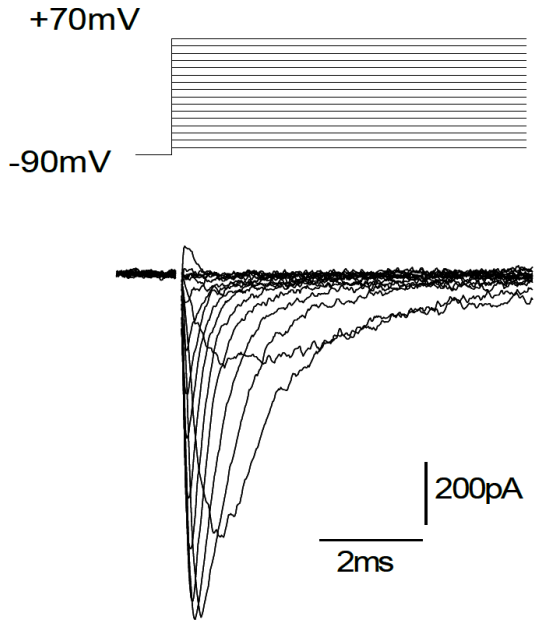

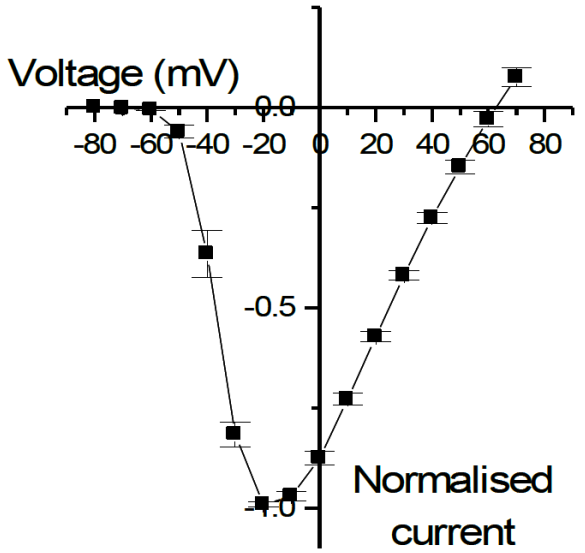

BACK

<u>hNa$_V$1.1 Raw Data Currents and Current-Voltage Relationship.</u> Membrane currents **(Left)** were elicited by the voltage protocol shown above the currents. **Right:** Mean current-voltage relationship (± S.E.M, n=9). (Manual Patch Clamp Data

$Na_V1.1$

BACK

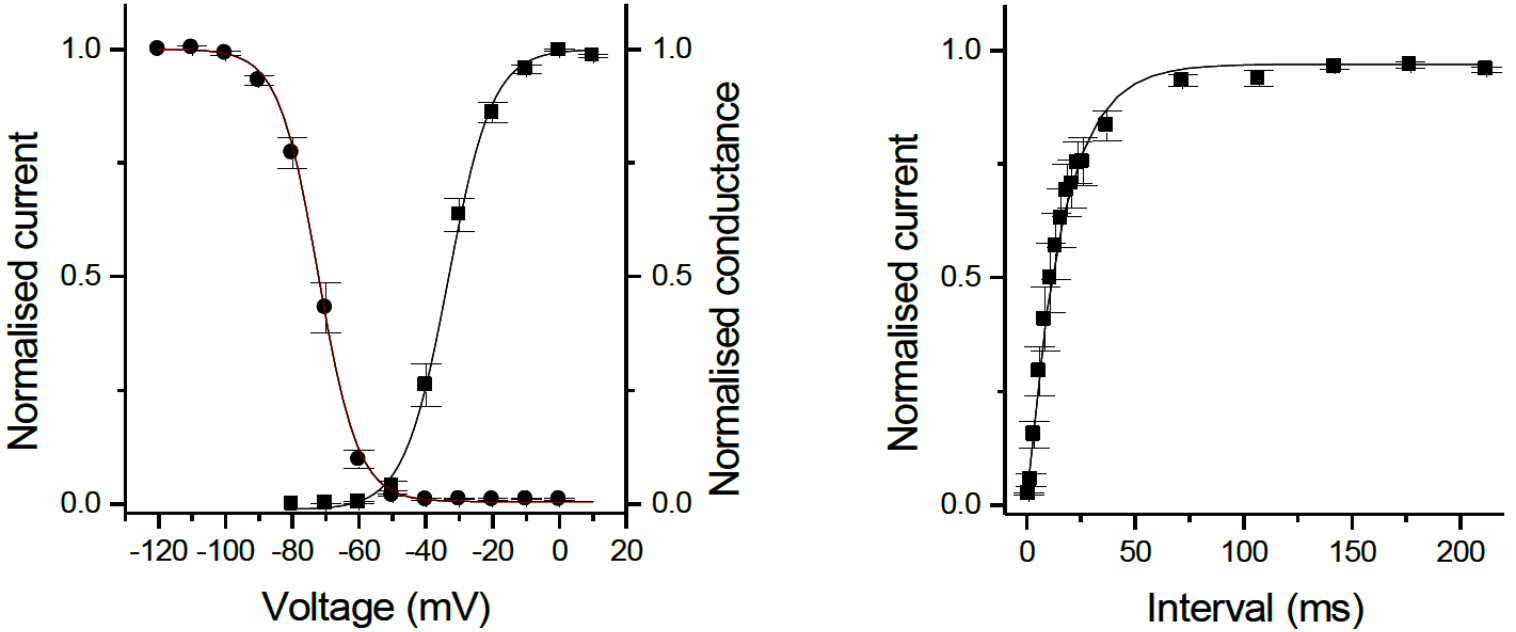

Voltage Dependence of Activation and Inactivation, Recovery from Inactivation. **Left:** Voltage dependence of activation (■) and inactivation (●) fitted to single Boltzmann functions. Conductance values were calculated from the current-voltage data and normalized to peak activation (mean ± S.E.M, n=9). Inactivation data was generated by applying a 1000 ms conditioning pulse, followed by a test pulse to 0 mV. The plot shows current, normalized to that evoked when a conditioning pulse of –120 mV was applied, against conditioning pulse potential (mean ± S.E.M, n=13). **Right:** Recovery from inactivation. Inactivation was generated by a 100 ms conditioning pulse, followed by a 100 ms conditioning pulse to 0 mV, followed by a test pulse at intervals thereafter. The current evoked by the test pulse was normalized to that evoked by the preceding conditioning pulse and plotted against the recovery interval (mean ± S.E.M, n=4). (Manual Patch Clamp Data).

$Na_V1.1$

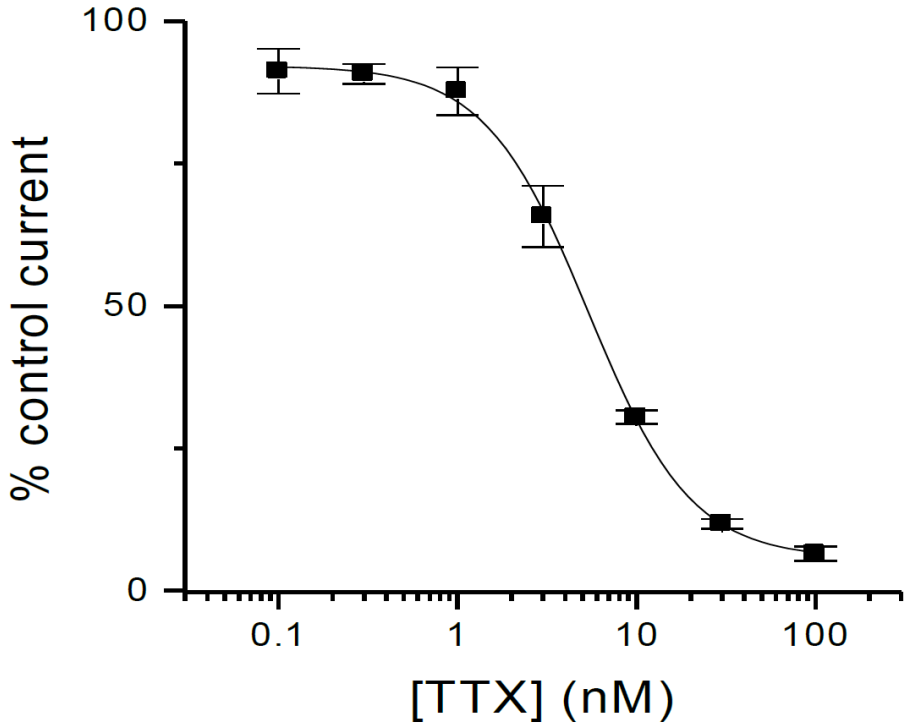

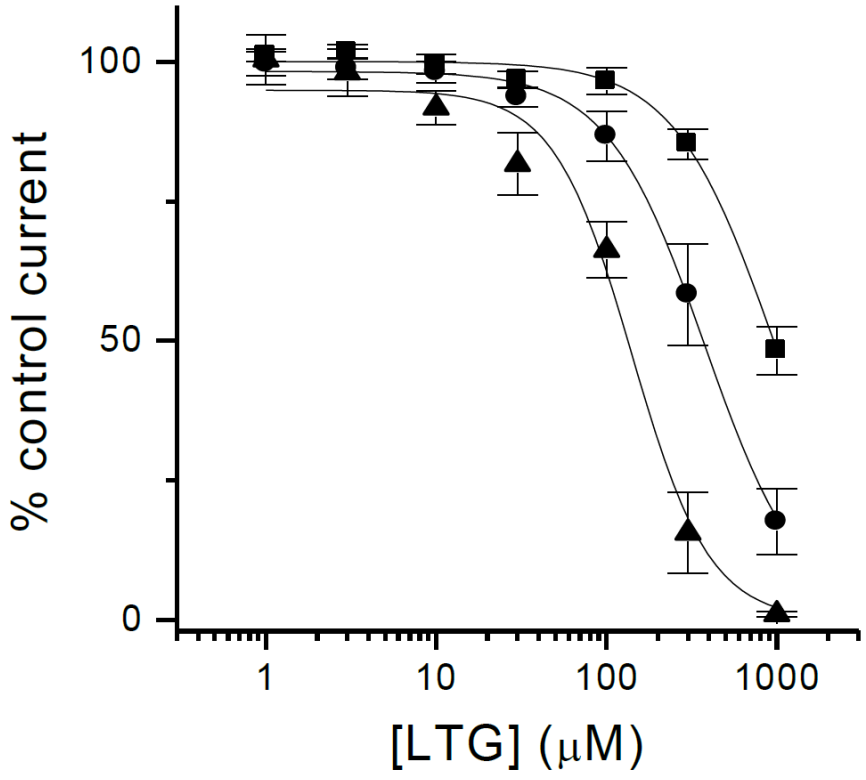

BACK

Pharmacology of hNaV1.1 currents. Left: Concentration-response relationship for tetrodotoxin (TTX). The curve was fitted with an independent binding site receptor model with an IC_{50} of 5.9 nM (n=4). Data presented normalized to the current elicited in the absence of TTX (mean ± SEM). **Right:** Concentration- and voltage-dependent inhibition by lamotrigine (LTG, lamictal). Concentration response curves were constructed from different holding potentials (VH). IC_{50} values of 950 µM (n=4), 377 µM (n=4) and 128 µM (n=4) for V_H of -120 (■), -90 (●) and –70 mV (▲) respectively. Data presented normalized to the current elicited in the absence of lamotrigine at each V_H (mean ± SEM, n=4). (Manual Patch Clamp Data).

$Na_V1.2$ (CYL3023)

BACK

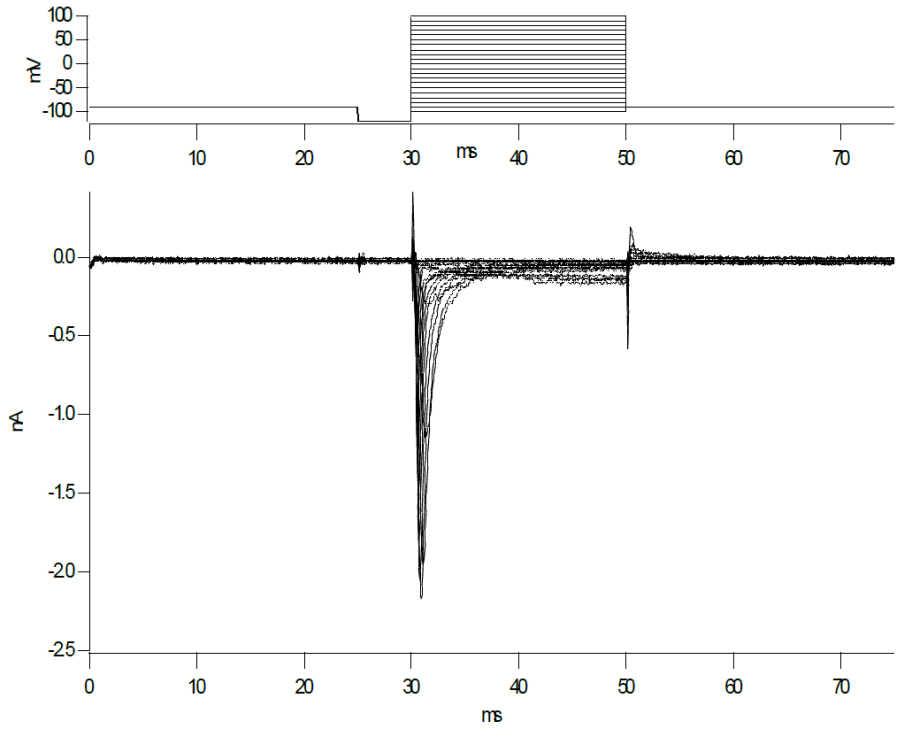

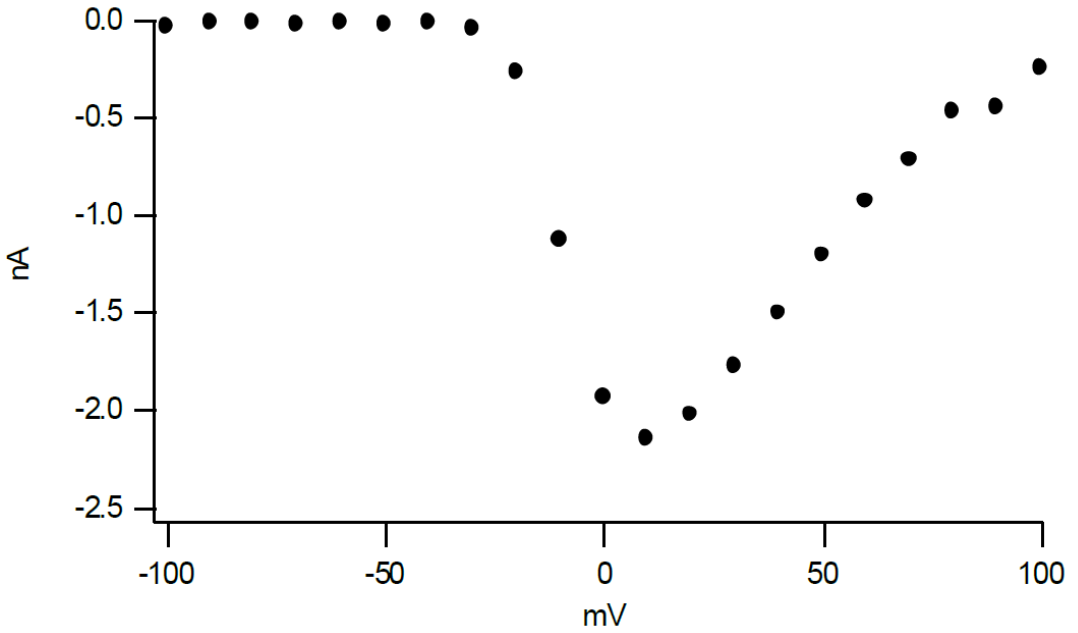

<u>hNa$_V$1.2 Raw Data Currents and Current-Voltage Relationship.</u> Membrane currents **(Left)** were elicited by the voltage protocol shown above the currents. **Right:** Current-Voltage relationship. (Manual Patch Clamp Data

$Na_V1.2$

BACK

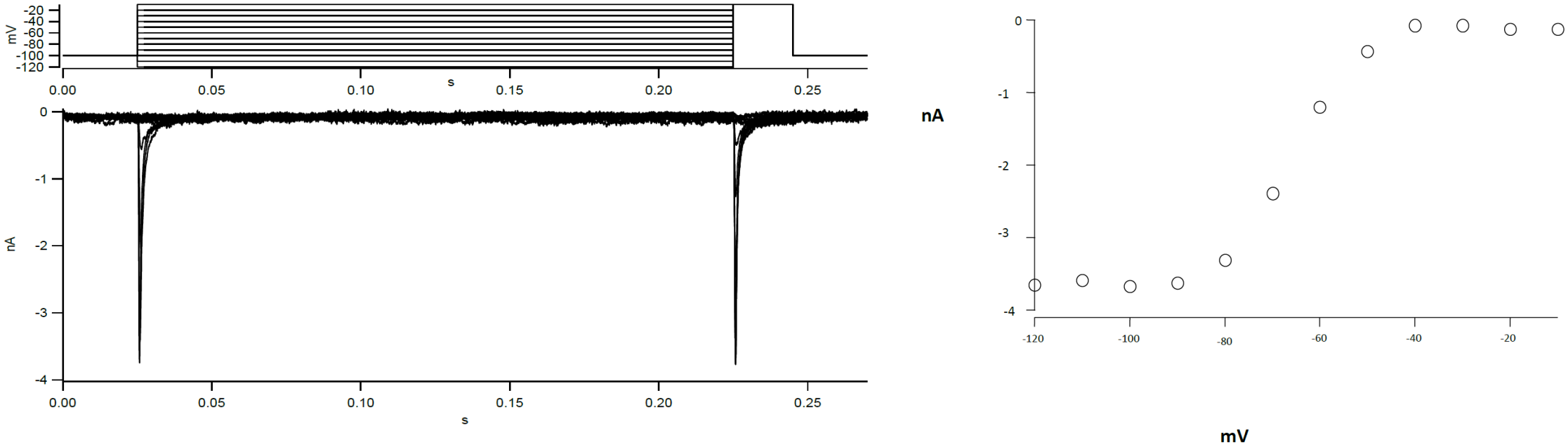

<u>Steady State Inactivation of hNa$_V$1.2 currents.</u> Left: Voltage protocol: voltage stepped to various pre-pulse potentials for 200 ms from a holding potential of -100 mV and then to a fixed test potential of -10 mV. **Right:** Peak inward Nav current at this test potential plotted against the pre pulse potential to obtain an estimate of the half steady state activation (V½ ~-65 mV) (Manual Patch Clamp Data).

$Na_V1.2$

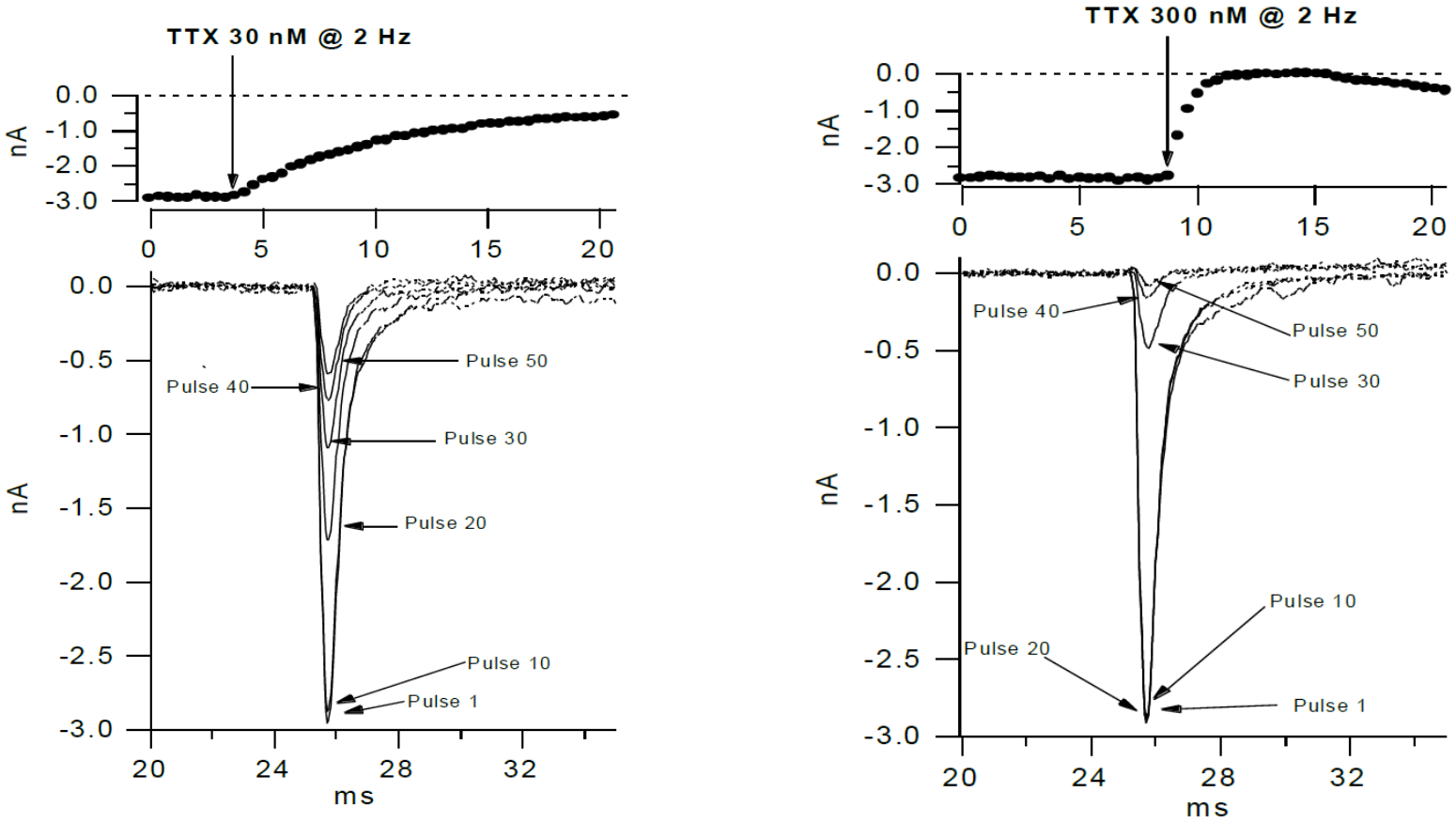

BACK

TTX Blockade of $hNa_V1.2$ currents. The block by TTX was examined at a fixed frequency of 2 Hz . Under these conditions, the estimated IC_{50} was 6.5 nM (Manual Patch Clamp Data).

$Na_V1.2$

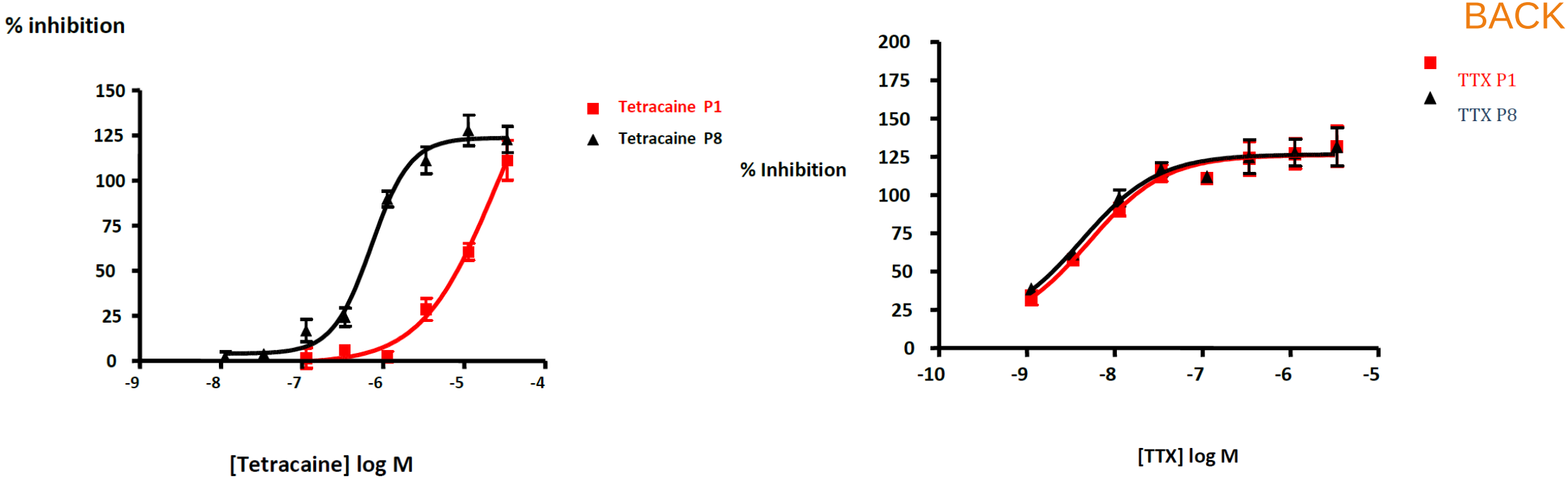

Use-Dependent Block of hNaV1.2 currents. Blockade of currents in a use dependent manner by Tetracaine **(Left)**, and lack of use-dependent blockade by TTX **(Right)**. Blockade was assessed at the 1st and 8 pulse delivered in 8-pulse trains. Voltage steps in the pulse trains were from -100mV to -10 mV antagonists. (IonWorks Quattro Data).

$Na_V1.3$ (CYL3003)

BACK

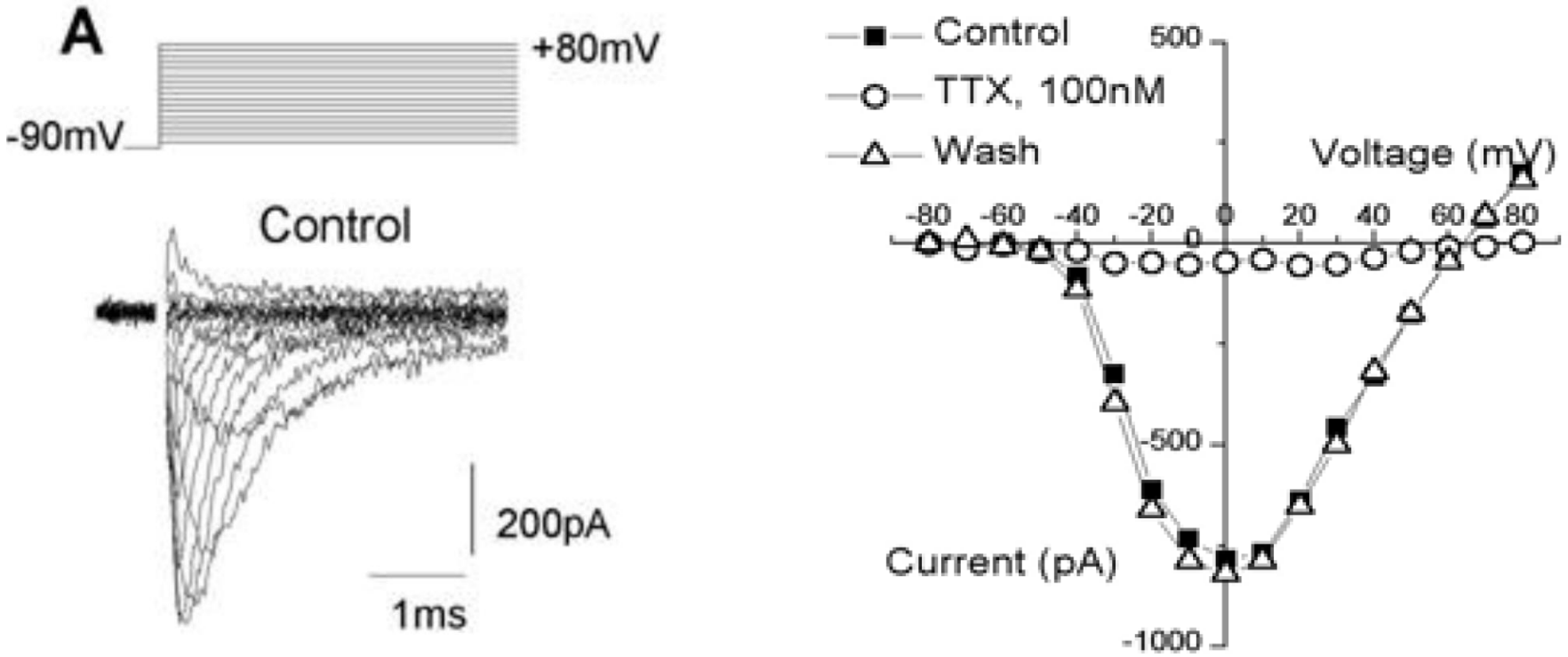

hNa$_V$1.3 Raw Data Currents and Current-Voltage Relationship. Representative currents **(Left)** elicited by a series of depolarising pulses given in 10 mV increments from the holding potential of -90 mV. **Right:** Current-Voltage relationship, Greater than 95% of the current is reversibly inhibited by TTX (100 nM) and an IC50 of 4 nM (4-5 nM, n=6) was calculated from the concentration response curve (Manual Patch Clamp Data).

$Na_V1.3$

BACK

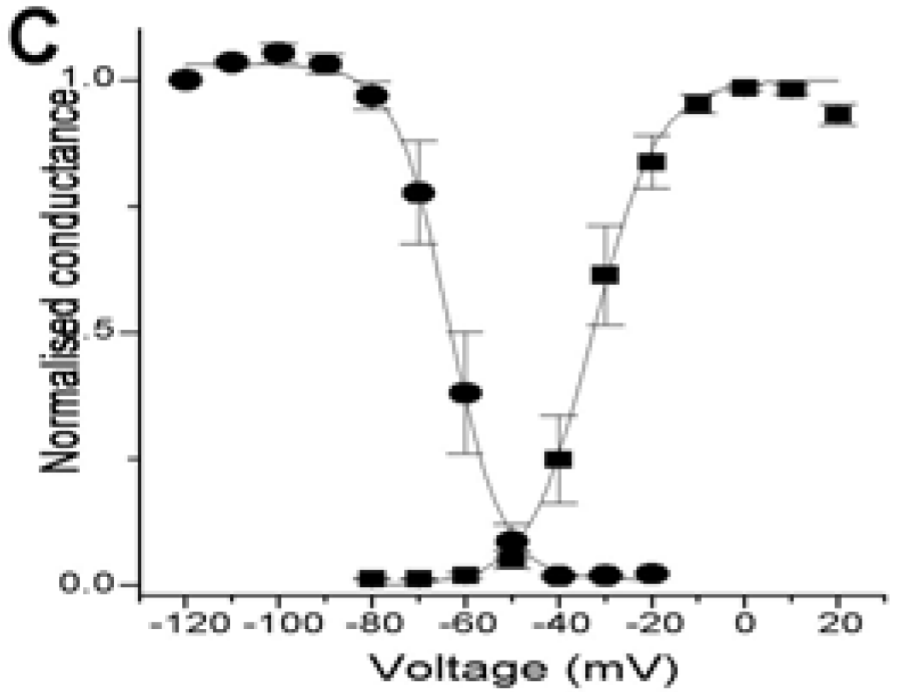

$hNa_V1.3$ activation and inactivation properties. The voltage-dependence of activation was calculated from the current-voltage relationship (G=I/(V-Erev)). The voltage-dependence of inactivation was measured by applying a conditioning pulse (1 sec) to varying potentials, from –120 to +20 mV, followed immediately by a test pulse to 0 mV. In both cases the curves were fitted to a Boltzman function, giving a half-activation potential of -23 ± 3 mV (n=11) and a half-inactivation potential of -69 ± 1 mV (n=13) (Manual Patch Clamp Data).

$Na_V1.3$

BACK

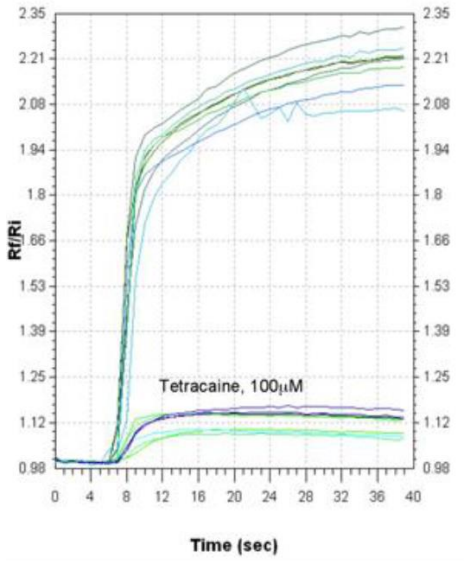

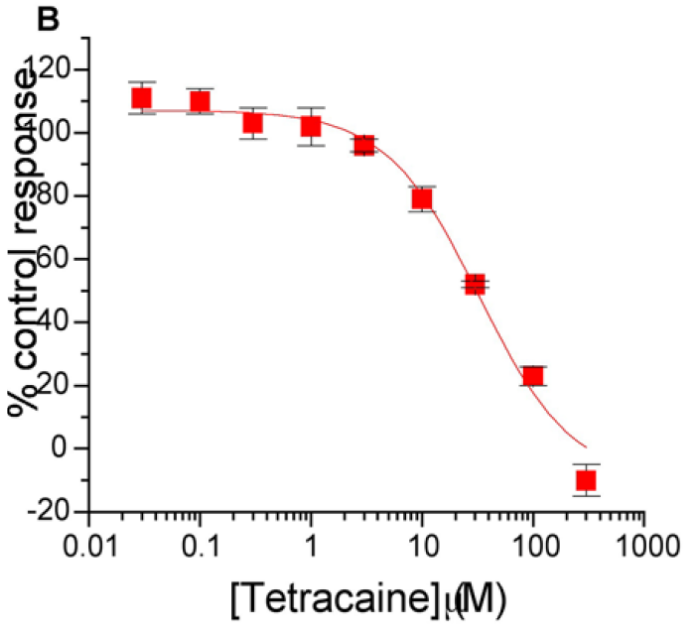

TTX Blockade of $hNa_V1.3$ channels. Left: In the presence of VSP fluorescent dyes (voltage sensitive probes) and scorpion venom, rapid, Na+ ion-dependent membrane potential depolarisations (indicated by an increase in the relative ratio of fluorescence from the 2 VSP dyes) are observed in hNav1.3-CHO K1 cells. These are significantly greater than in untransfected controls (not shown) and are blocked with tetracaine. **Right:** Concentration dependent inhibition of VIPR responses by the local anesthetic, tetracaine (IC50 = 32 mM). (VIPR Data).

$Na_V1.4$ (CYL3024)

BACK

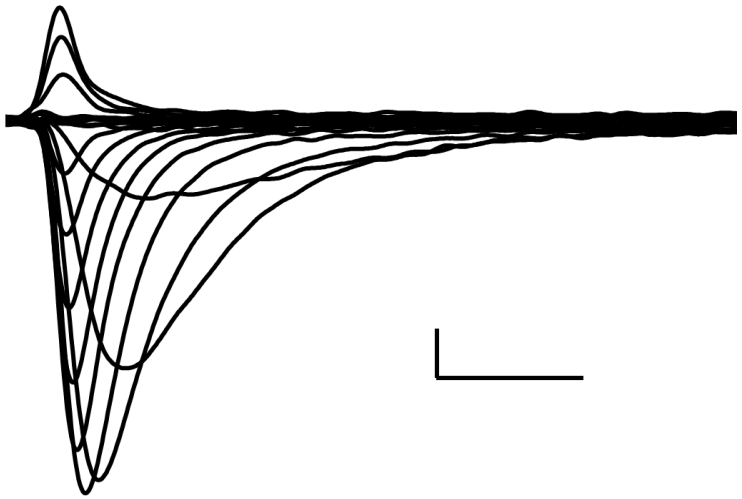

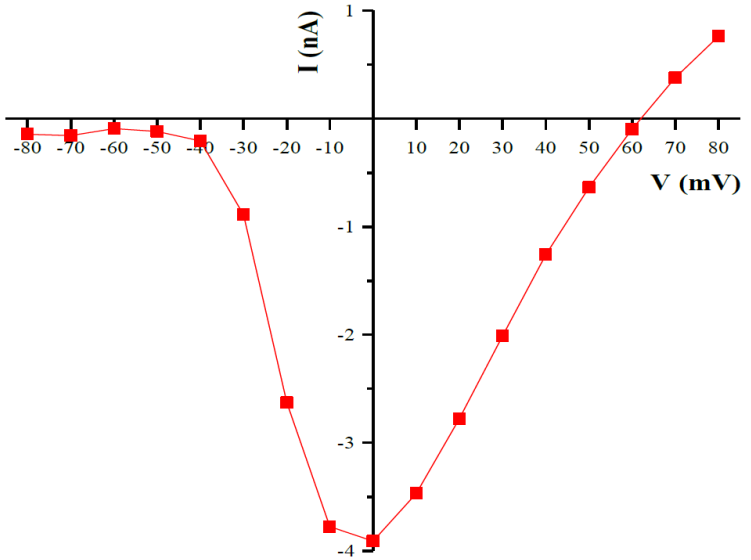

$hNa_V1.4$ Raw Data Currents and Current-Voltage Relationship. The currents **(Left)** were produced by 25 ms voltage steps from –80 mV to +80 mV in 10 mV increments following a conditioning pulse of –120 mV for 100 ms. Sweeps every 25 s. The cells were held at a holding potential of –80 mV. Scale bars represent 1 ms and 500 pA. **Right:** Current-Voltage relationship (Manual Patch Clamp Data).

$Na_V1.4$

BACK

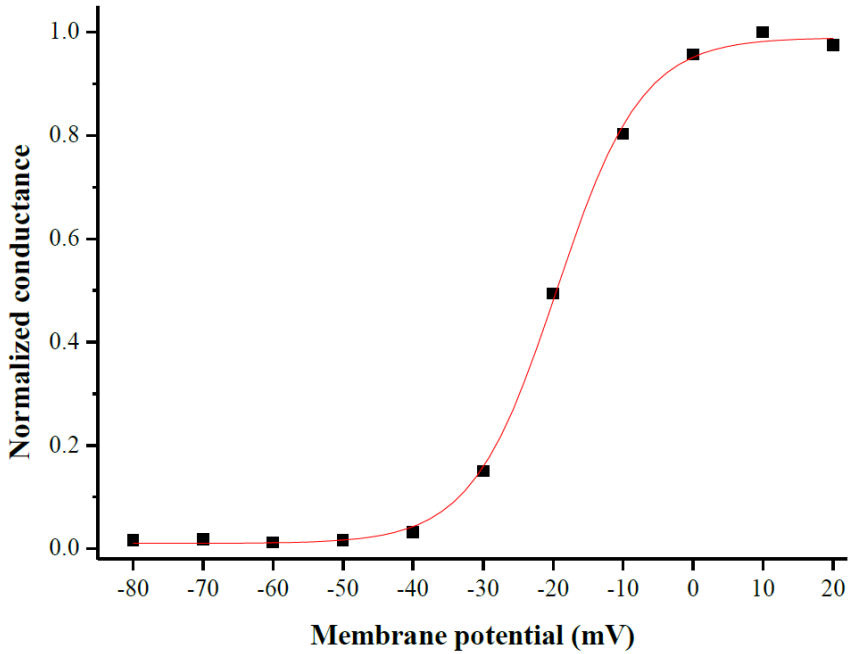

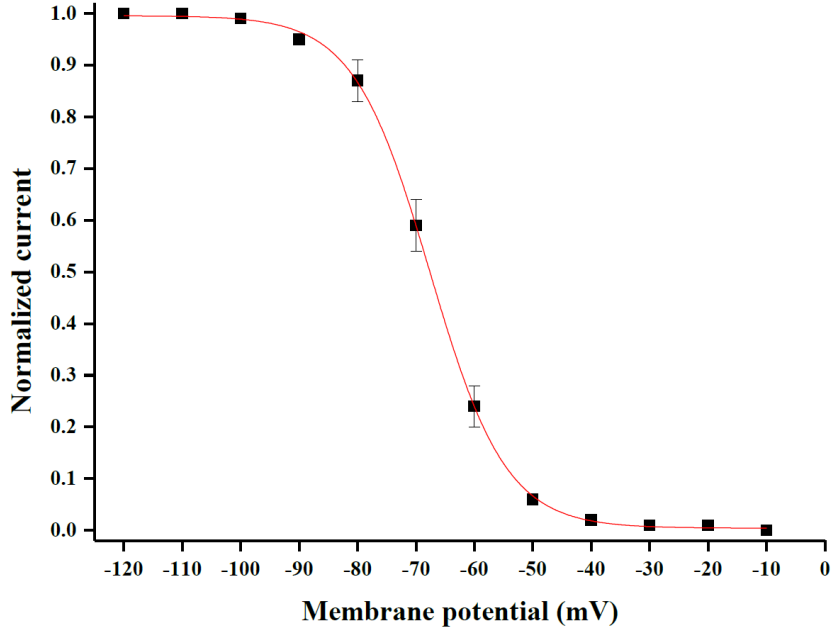

<u>$hNa_V1.4$ Activation and Inactivation Properties.</u> **Left:** The conductance was normalized to peak conductance at +10 mV and plotted against membrane voltage. The data could be described by a Boltzmann equation with a V½ = -19.5 ± 0.3 mV and k = 6.1 ± 0.3. **Right:** The hNav1.4 channel had a half-inactivation voltage ($V_{1/2}$) of approximately –68 mV and a slope (k) of 6.2 ± 0.3 (Manual Patch Clamp Data).

$Na_V1.4$

BACK

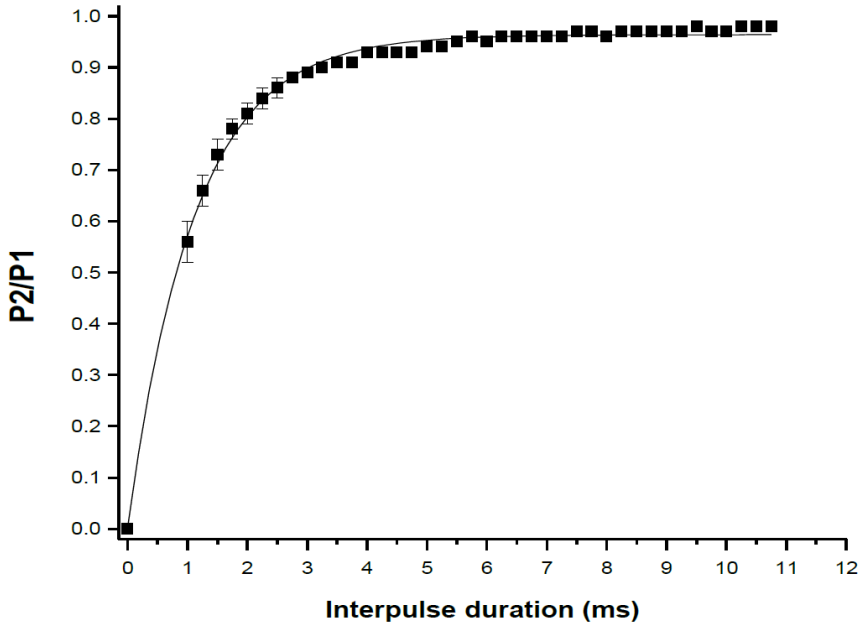

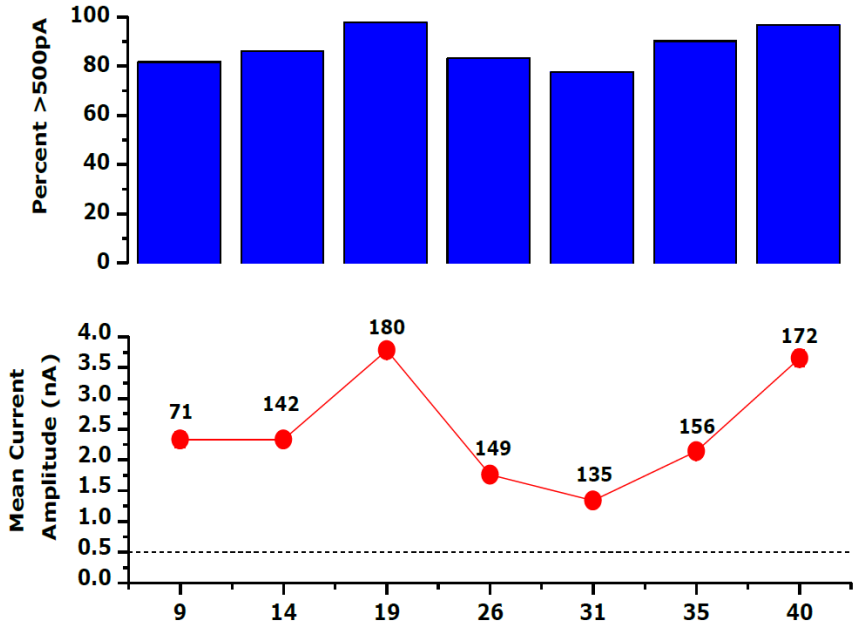

<u>hNa$_V$1.4 Recovery from Inactivation, and Stability of Expression.</u> Left: A double pulse protocol was used, the membrane was first stepped from the holding potential of -80 mV to -120mV for 500 ms, then to -10 mV for 25ms (pulse 1). Immediately after the step to -10 mV the voltage was returned to -120 mV for varying amounts of time ranging from 1 – 10.75 ms in 0.25 ms intervals (interpulse duration), then back to -10 mV (pulse 2), (Manual Patch-Clamp Data). **Right:** The upper panel shows the percentage of cells expressing a mean peak inward current >500 pA for cell passages 9, 14, 19, 26, 31, 35 and 40. The lower panel shows the mean current amplitude (mean ± SEM, red circles) and the number of these cells above the red circles. (IonWorks HT Data)

$Na_V1.4$

BACK

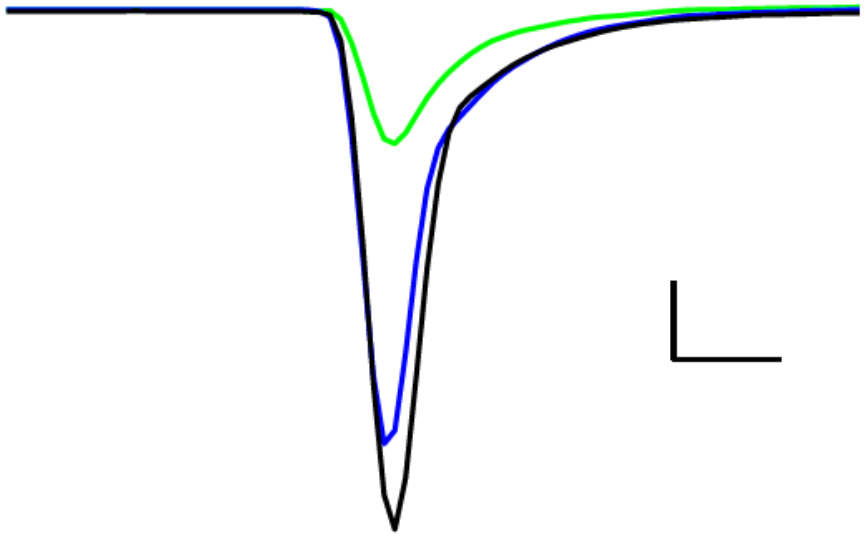

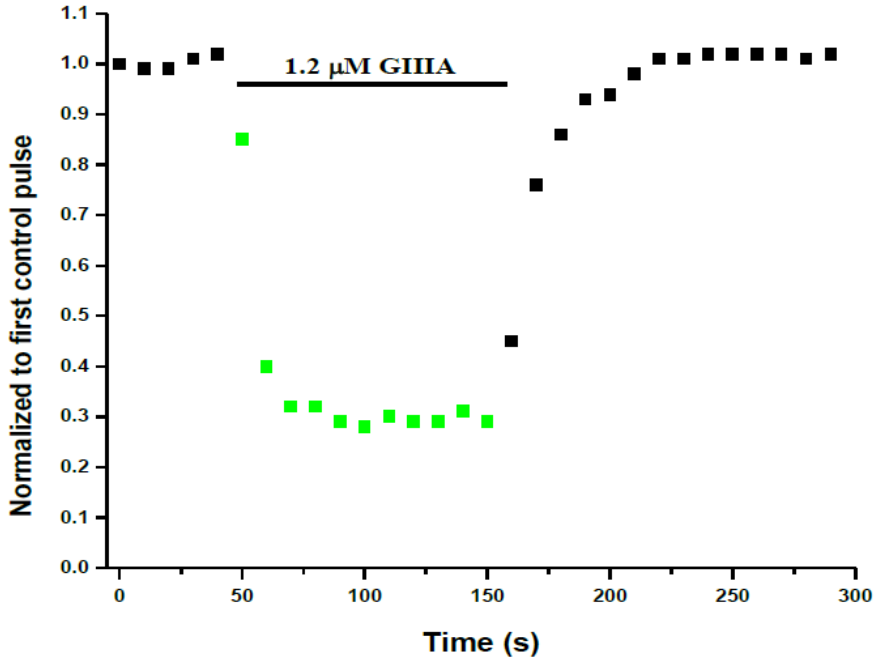

hNa$_V$1.4 Pharmacology. Left: Typical traces showing the effect of 1.2 µM µ-conotoxin GIIIA. Sodium currents are shown before (black trace), in the presence of (green trace) and after washout (blue trace) of µ-conotoxin GIIIA. The cells were held at a holding potential of –80 mV and then stepped to –120 mV for 5 ms followed by a test pulse to –30 mV for 20 ms. Sweeps every 10 s. Scale bars represent 1 ms and 2 nA. **Right:** Typical example of the effect of 1.2 µM µ-conotoxin GIIIA. The currents were normalized to the peak current at time, mean inhibition was 65 ± 5.1 percent (n =4) (Manual Patch Clamp Data)

$Na_V1.5$ (CYL3004)

BACK

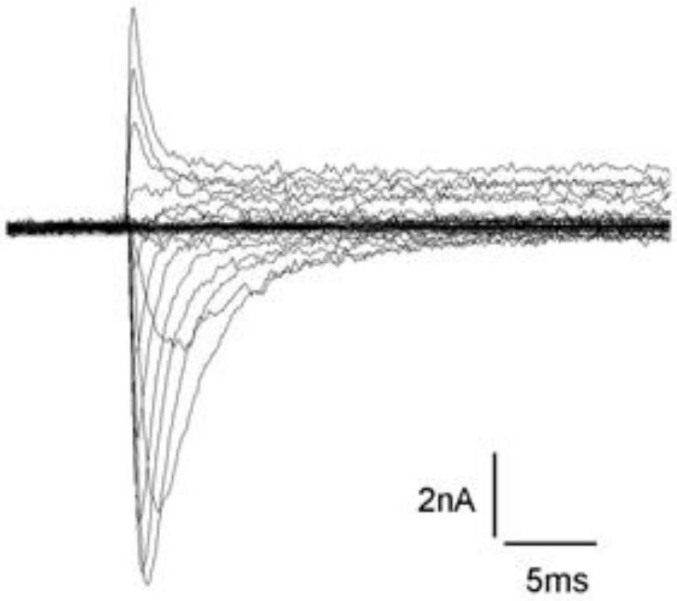

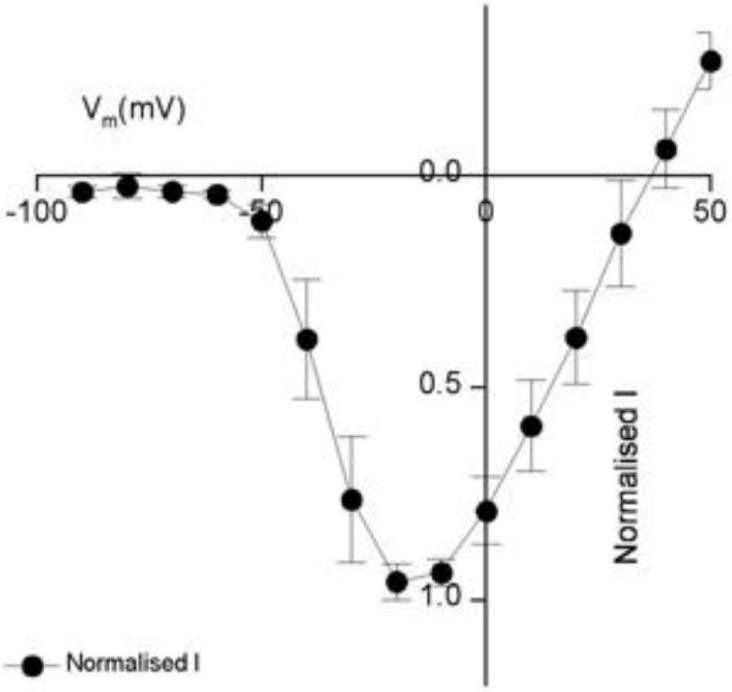

<u>$hNa_V1.5$ Raw Data Currents and Current-Voltage Relationship.</u> The currents **(Left)** were produced by 25 ms voltage steps from –80 mV to +80 mV in 10 mV increments following a conditioning pulse of –120 mV for 100 ms. Sweeps every 25 s. The cells were held at a holding potential of –80 mV. Scale bars represent 1 ms and 500 pA. **Right:** Current-voltage (I/V) relationship (Manual Patch Clamp Data).

$Na_V1.5$

BACK

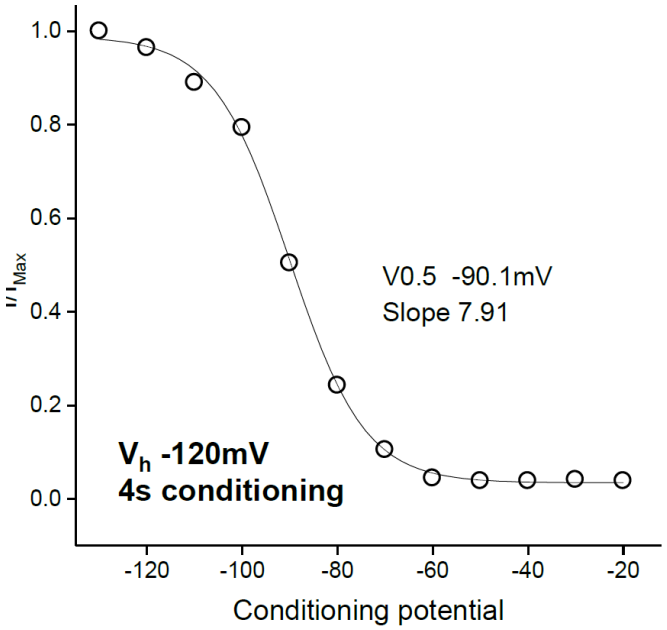

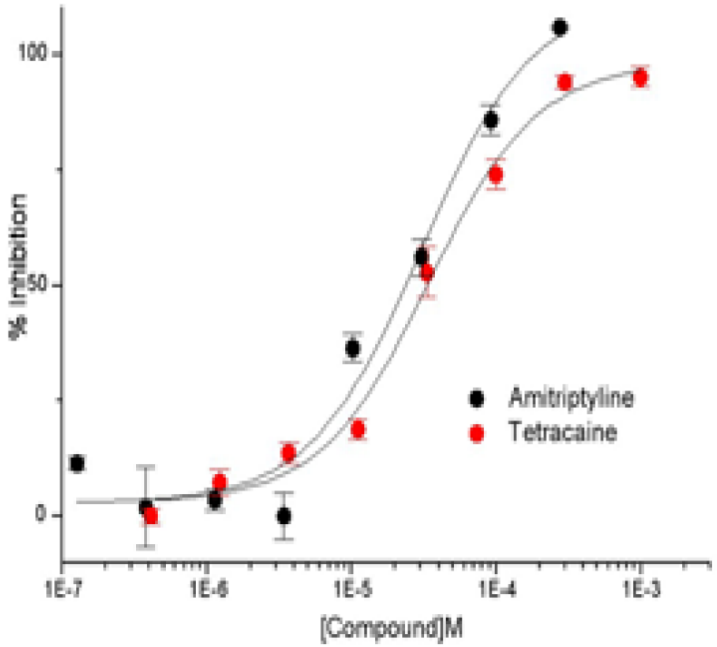

hNa$_V$1.5 Activation and Inactivation properties. **Left:** The conductance was normalized to peak conductance at +10 mV and plotted against membrane voltage. The data could be described by a Boltzmann equation with a V½ = -19.5 ± 0.3 mV and k = 6.1 ± 0.3 (Manual Patch Clamp Data). .
Right: The hNav1.4 channel had a half-inactivation voltage ($V_{1/2}$) of approximately –68 mV and a slope (k) of 6.2 ± 0.3 (FLIPR Data).

$Na_V1.5$

BACK

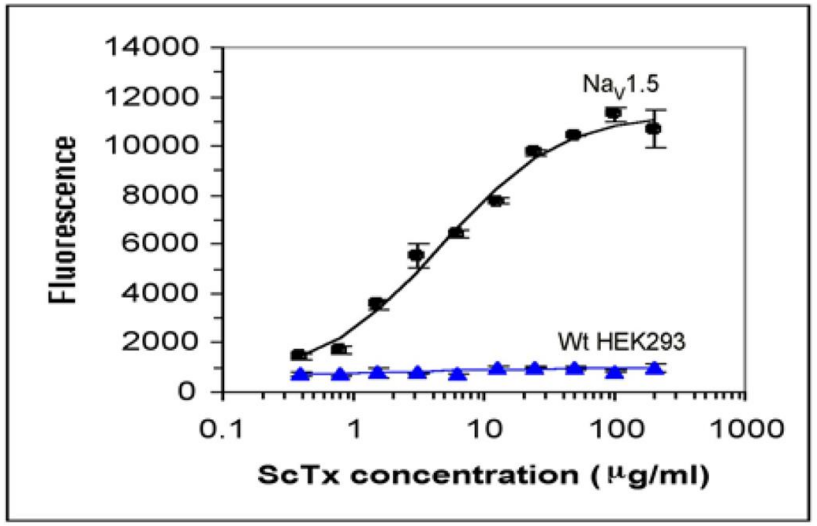

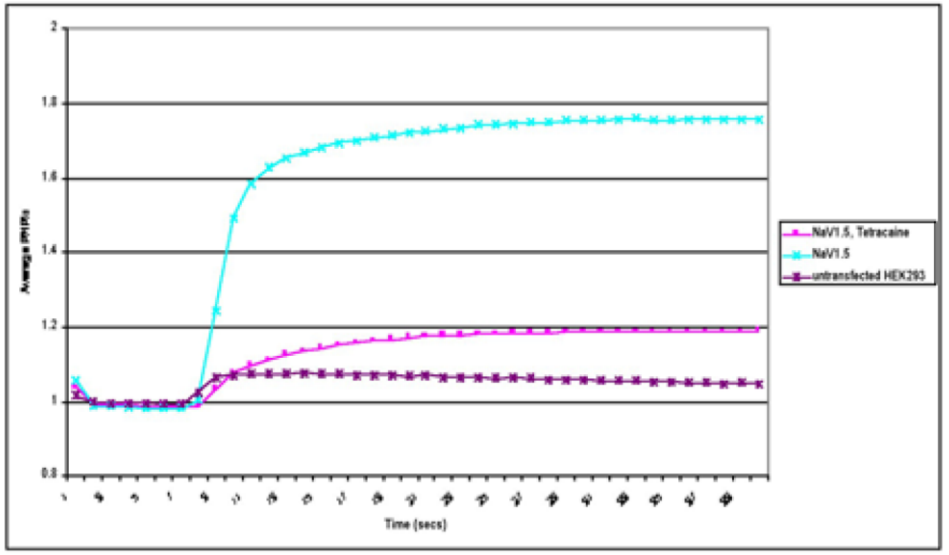

hNav1.5 Cell Line in Fluorescent Screening Assays. Left: cells incubated with DiBAC and scorpion venom (ScTx), KCl induces reproducible membrane potential depolarizations (increased fluorescence) that are dependent in size upon the concentration of ScTx used. No responses are seen in untransfected HEK293 cells (FLIPR Data). **Right:** In hNav1.5-HEK expressing cells incubated with VSP fluorescent dyes (voltage sensitive probes) and scorpion venom, a rapid Na+ ion-dependent membrane potential depolarizations (increase in the relative ratio of fluorescence from the 2 VSP dyes) are observed. These are significantly greater than in untransfected controls and can be blocked with the standard inhibitor tetracaine. (VIPR Data).

$Na_V1.6$ (CYL3010)

BACK

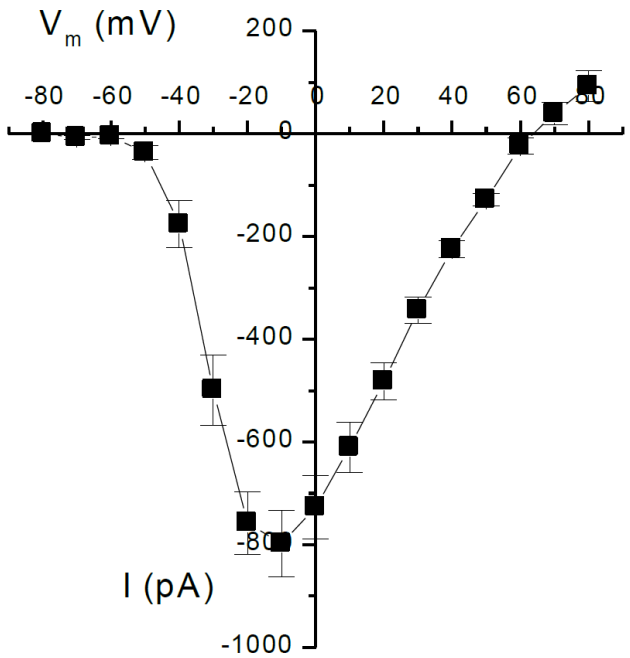

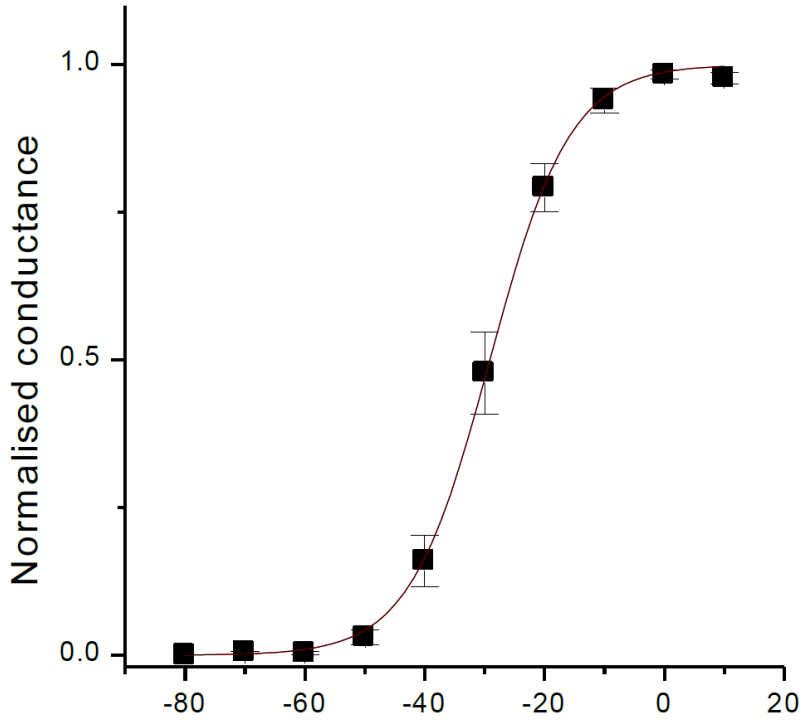

hNa$_V$1.6 Current-Voltage (I/V) and Conductance-Voltage G/V relationships. The current-voltage relationship **(Left)** from 9 cells were plotted as the average currents as a function of the test pulse potentials. **Right:** Voltage-dependence of activation calculated from the current-voltage relationship. The conductance was calculated by dividing the peak current by the driving force, based upon an observed reversal potential. The half maximal activation was determined as -29.2 ± 1.8 mV and the slope was 6.0 ± 0.2 (n=9). (Manual Patch Clamp Data).

$Na_V1.6$

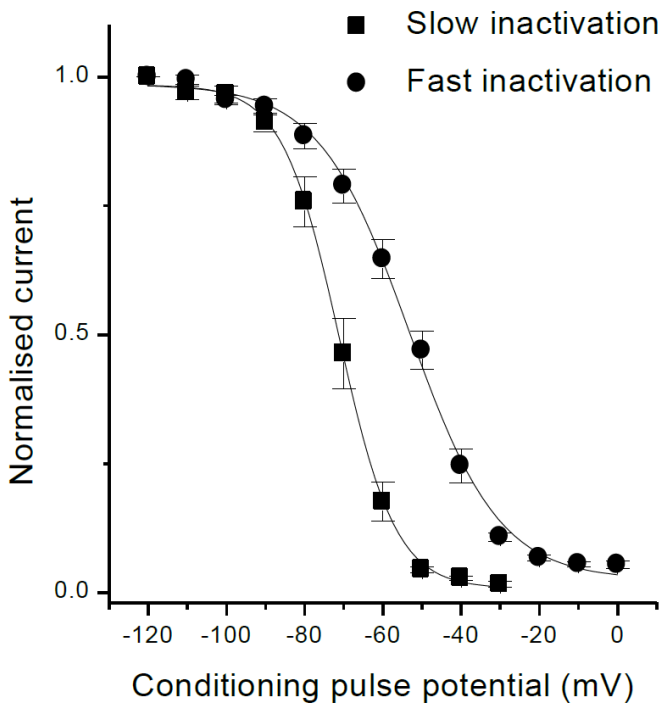

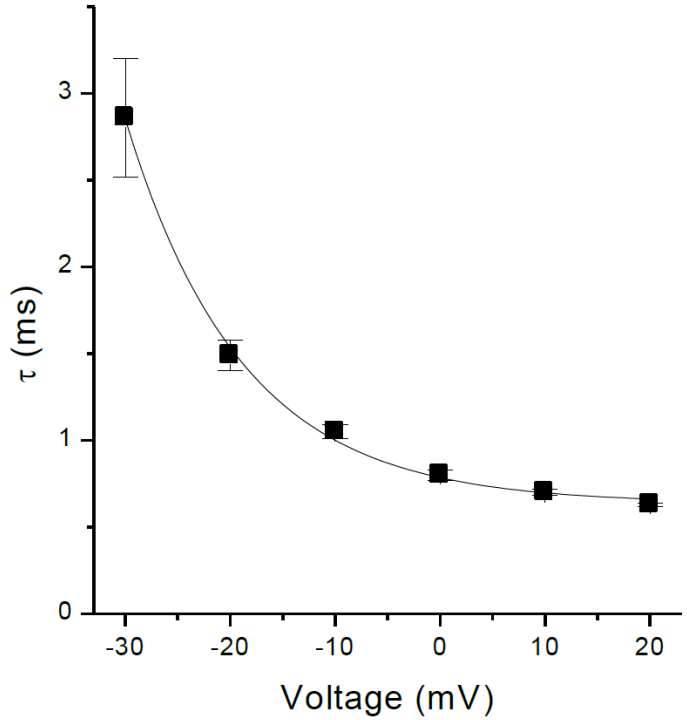

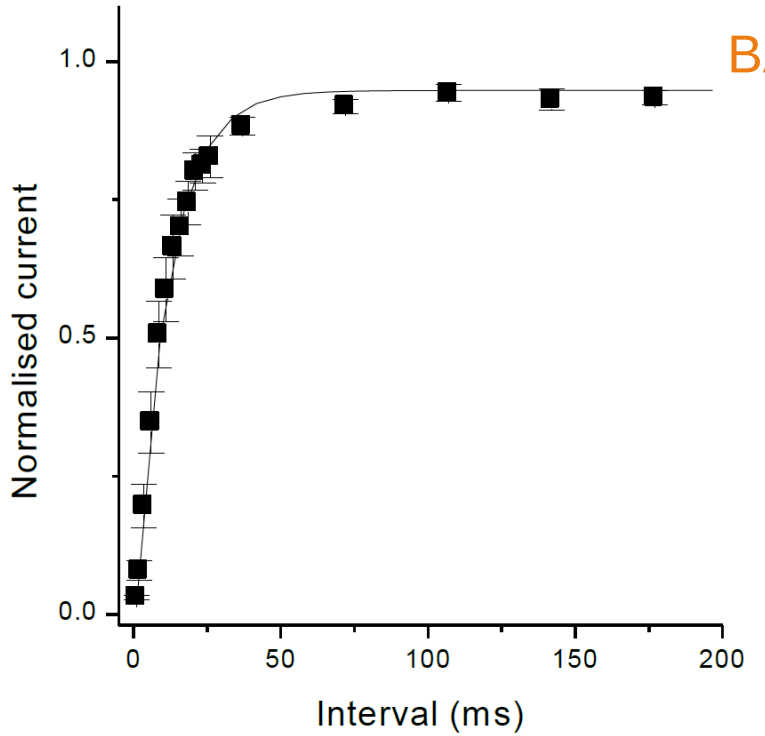

BACK

<u>hNa$_V$1.6 Inactivation Properties.</u> **Left:** Voltage-dependence of inactivation measured after conditioning pulses (10 mV intervals) of either 10 ms (fast inactivation) or 1 ms (slow inactivation) followed by a test pulse to 0 mV. Peak currents elicited by the test pulse was normalised to the current evoked when a conditioning pulse of –120 mV was used. The curves were fitted with a Boltzmann function and the half maximal voltages for fast and slow inactivation were determined as -53.4 ± 2.0 mV (n=9) and -71.6 ± 1.9 mV (n=9), respectively. The slopes were 11.6 ± 0.6 (n=9) for fast inactivation and 6.5 ± 0.3 for slow inactivation. **Middle:** Time constants (τ) of inactivation as a function of test pulse potential. The τ values were determined by fitting a single exponential function to the decay phase of the currents. **Right:** Recovery from inactivation. Currents and subsequent inactivation were evoked by 100 ms conditioning pulses to 0 mV followed by various intervals at –90 mV, before test pulses to 0 mV. The currents were normalized to that evoked by the preceding conditioning pulse and plotted as a function of recovery interval. A single exponential function was fitted to the data and a time constant of 12.6 ± 2.0 ms (n=6) was determined. (Manual Patch Clamp Data).

$Na_V1.6$

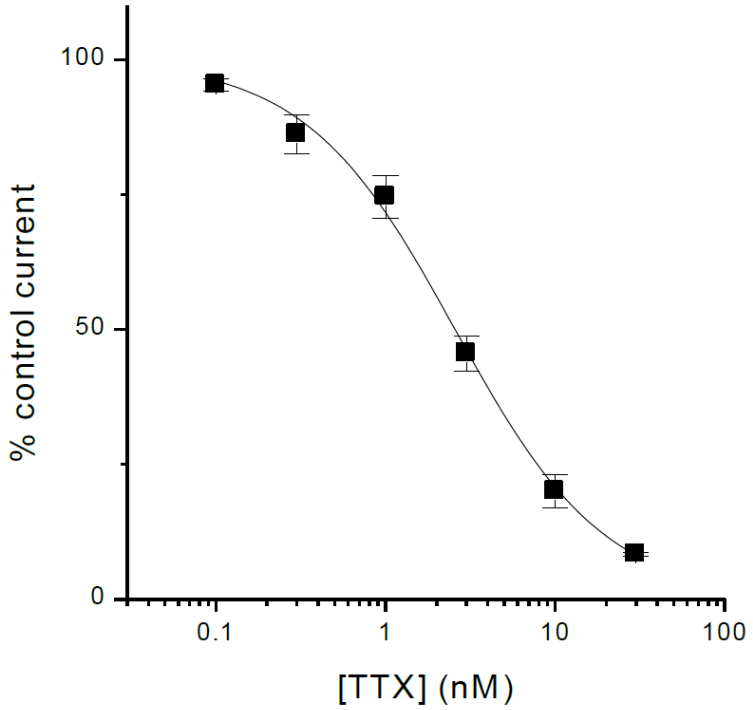

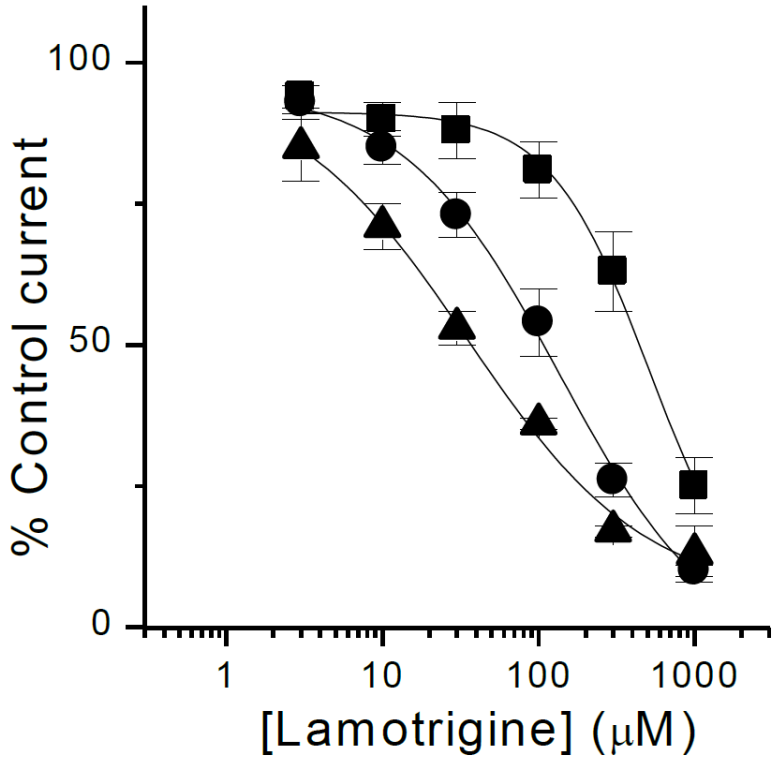

BACK

hNav1.6 Pharmacology. Left: Dose response curve for tetrodotoxin (TTX) inhibition of sodium currents in HEK293 cells stably expressing human Nav1.6 sodium channels. The curve was fitted with an independent binding site receptor model and the IC_{50} was calculated as 2.5 nM [1.9-3.4] with an nH of 1.04 ± 0.08 (n=7).ells incubated with DiBAC and scorpion venom (ScTx), KCl induces reproducible membrane potential depolarizations (increased fluorescence) that are dependent in size upon the concentration of ScTx used. No responses are seen in untransfected HEK293 cells (FLIPR Data). **Right:** Concentration response curves for inhibition by Lamotrigine (Lamictal) at different holding potentials. IC_{50} Values were calculated as 486 μM [393-602], 127μM [63-254] and 31μM [19-49] at -120 (■), -90 (●) and -60mV (▲) respectively (n=4-7). (VIPR Data).

$Na_V1.7$ (CYL3011)

BACK

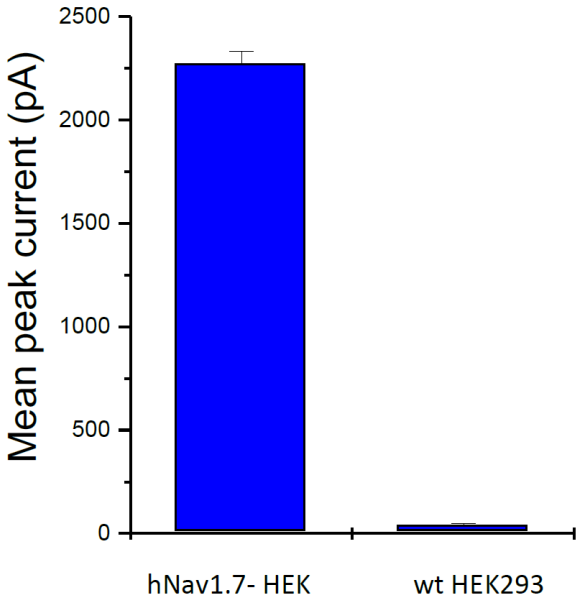

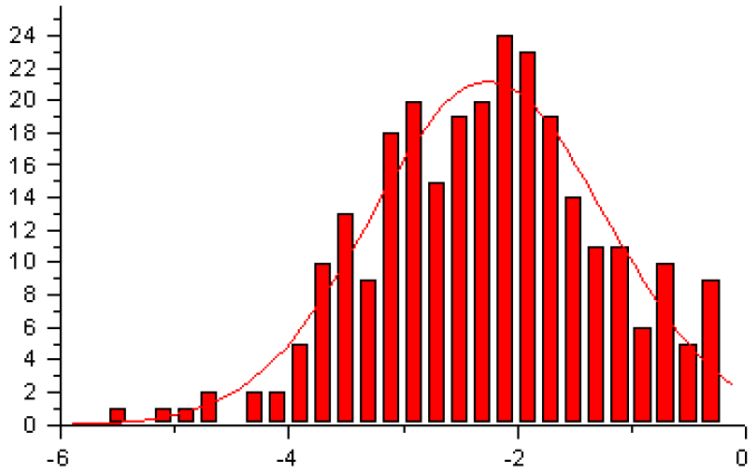

<u>hNa$_V$1.7 Mean Current and Current Amplitude Distribution.</u> Mean peak currents **(Left)** elicited by a depolarizing pulse to -10 mV from -100 mV [Na]ext = 68.5 mM (to reduce current amplitude) and HEK293 wild type cells [Na]ext = 137 mM). **Right:** Amplitude distribution of hNa$_V$1.7 currents ([Na]ext = 68.5 mM) (IonWorks HT Data).

$Na_V1.7$

BACK

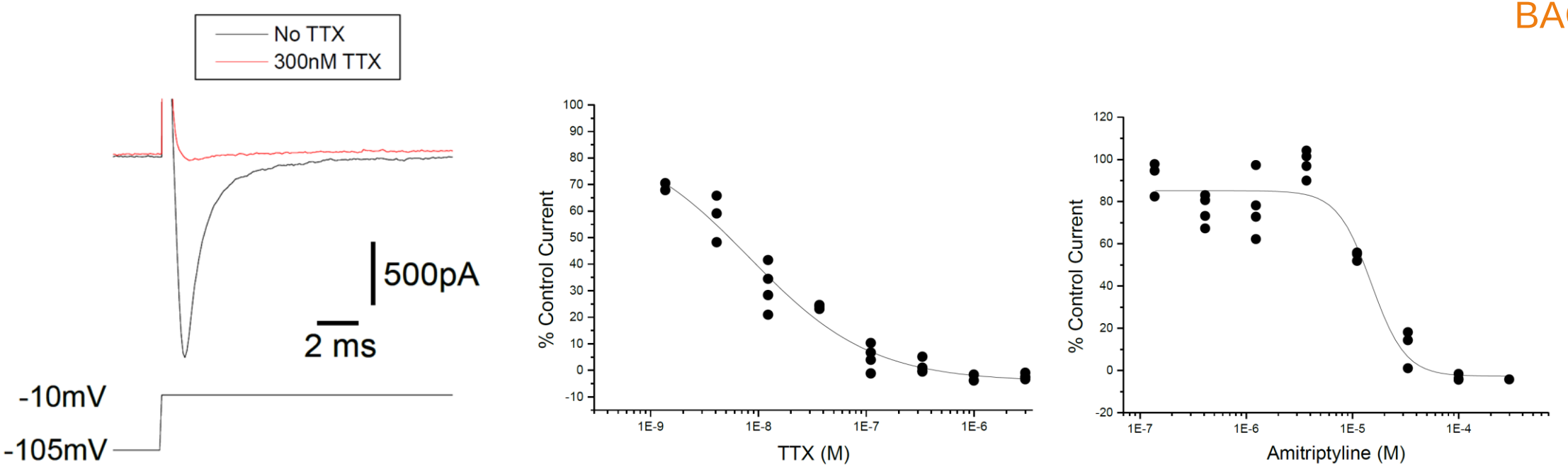

hNa$_V$1.7 Inactivation Properties. **Left:** Representative current elicited by a depolarising pulse to -10 mV from a holding potential of –105 mV on IonWorks HT electrophysiology platform. The current was blocked with 300 nM TTX. **Middle:** Representative concentration-response curves for inhibition of hNav1.7 currents by TTX **(Middle)** and amitriptyline **(Right).** Each point represents the value from single cell determinations (different cells). The mean IC50 values from multiple IonWorks HT dose response data analyses were 9 nM for TTX (n = 3) and 15.8 µM for amitriptyline (n=4) (IonWorks HT Data).

$Na_V1.8/\beta_1$ (CYL3025)

BACK

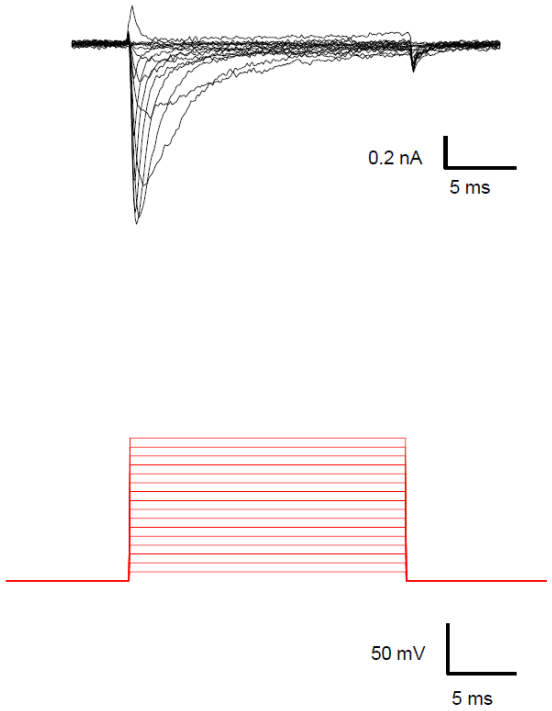

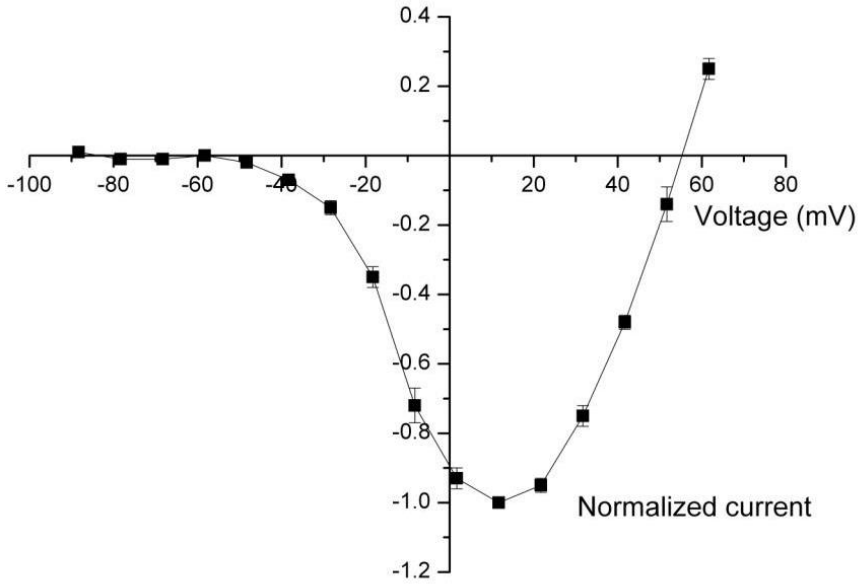

$hNa_V1.8/\beta_1$ Raw Data Currents and Current-Voltage Relationship. Typical current traces **(Left)** for $hNa_V1.8/\beta1$ evoked by depolarizing voltage steps. The currents were produced by 100 ms voltage steps from –90 to +60 mV in 10 mV increments. Sweep every 10 s. The cells were held at a holding potential of –90 mV. The voltage protocol used is shown in red. **Right:** Typical Current-voltage (I/V) relationship for $hNa_V1.8/\beta1$. (Manual Patch Clamp Data)

$Na_V1.8/\beta_1$

BACK

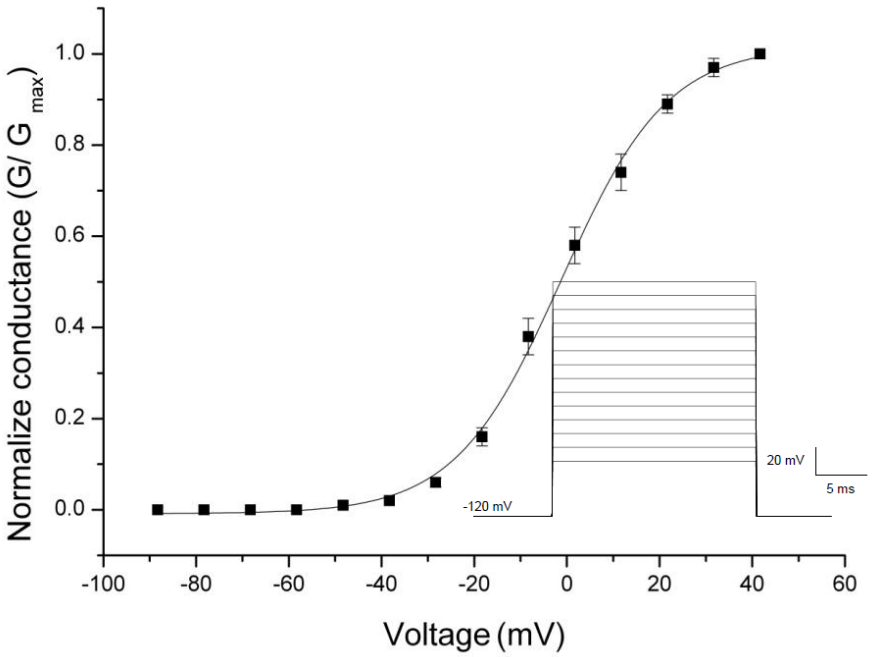

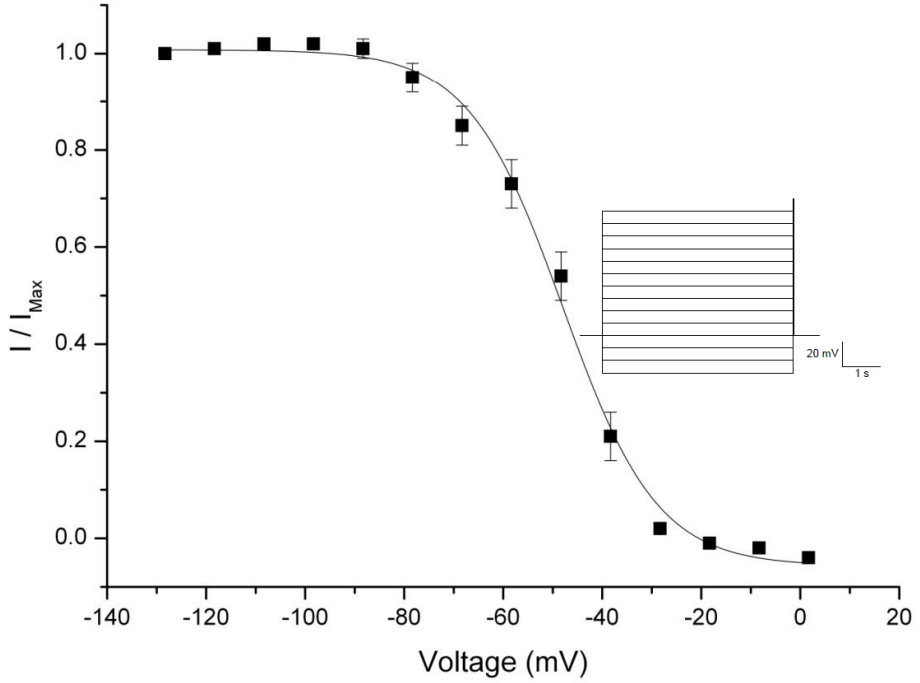

<u>$hNa_V1.8/\beta_1$ Activation and Inactivation Properties.</u> **Left:** Conductance-voltage (G/V) graph of the hNav1.8/β1 current. The conductance was normalized to peak conductance at +20 mV and plotted against membrane voltage. The voltage protocol used is shown (inset). **(Right).** Steady-state inactivation of the $hNa_V1.8/\beta1$. The voltage protocol used is shown (inset). (Manual Patch Clamp Data).

$Na_V1.8/\beta_1$

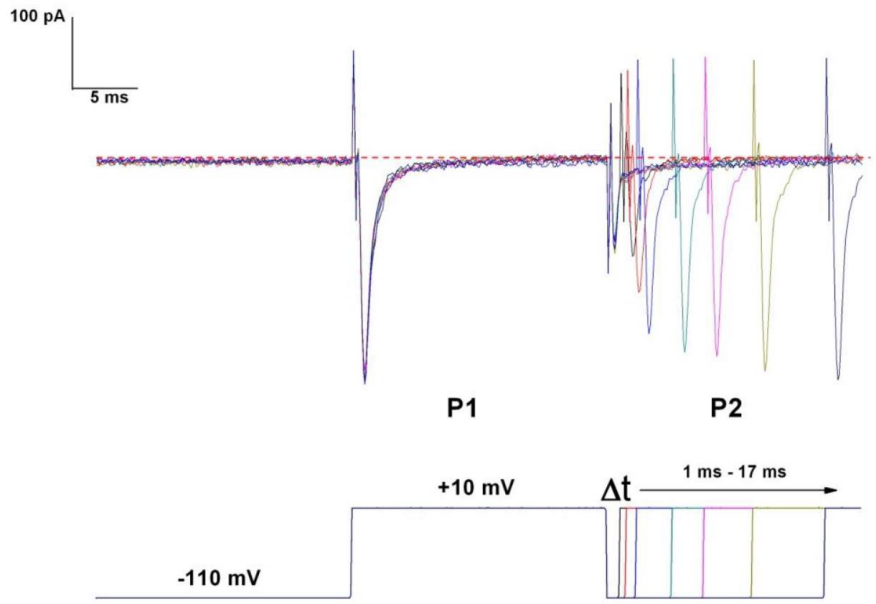

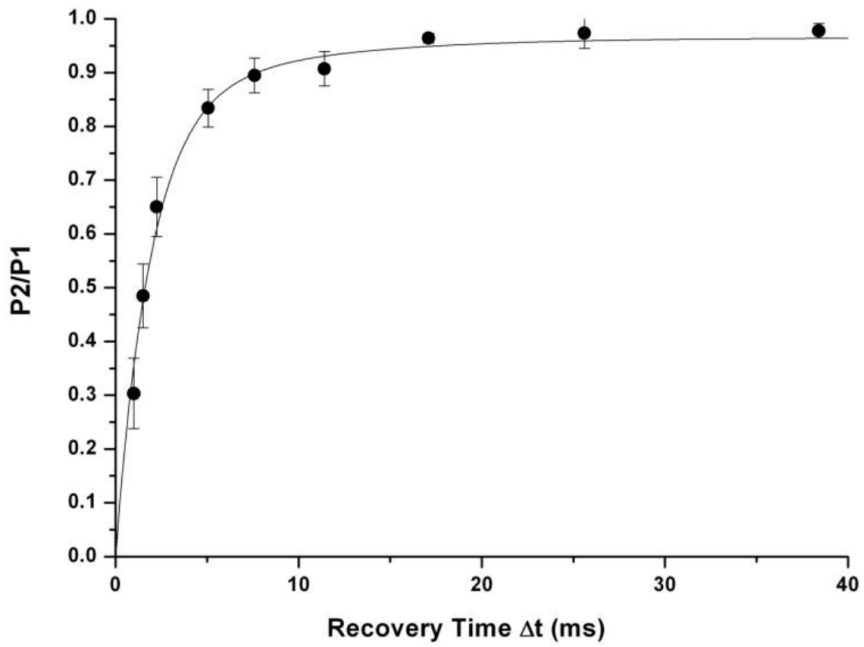

BACK

<u>$hNa_V1.8/\beta_1$ Recovery from Inactivation.</u> **Left:** In order to assess the time constant of recovery of inactivation at -110 mV following an inactivating 20 ms voltage step to 10 mV, a double pulse protocol was used. The membrane was first stepped from the holding potential (-110 mV) to 10 mV for 20 ms (Pulse 1, P1). Immediately after the step to 10 mV the voltage was returned to -110 mV for varying amounts of time ranging from 1 – 17 ms with each successive intervals increasing by 50% (interpulse duration). After each incremental change in time, the voltage was stepped back to 10 mV (Pulse 2, P2). The Pulse 2/Pulse 1 ratio is plotted in the graph **(Right)** for three cells, where P2/P1 is plotted against the relevant interpulse duration. The data could be described by a double exponential giving an estimated time constants of recovery where the predominant recovery time constant (approx 80% of total amplitude), τ_{fast} = 1.9 ± 0.4 ms and the slower time constant (20% of the amplitude), τ_{slow} = 8.2 ± 13.2 ms (Figure 5).

$Na_V1.8/\beta_1$

BACK

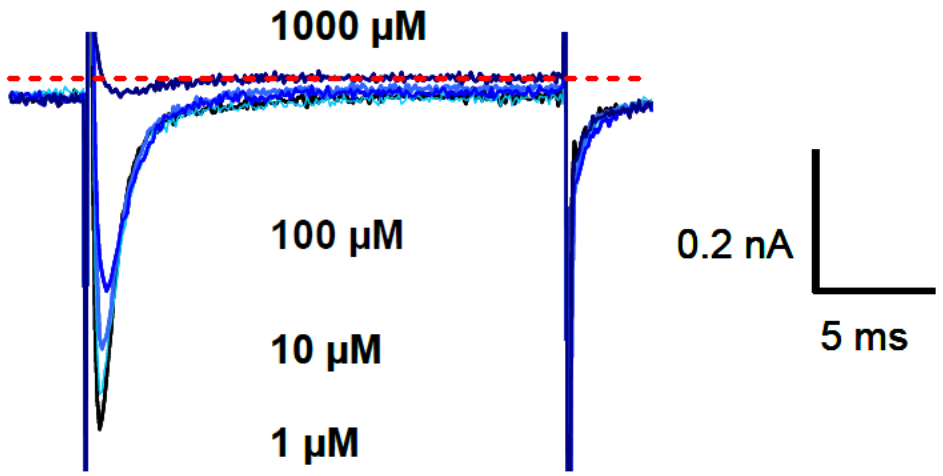

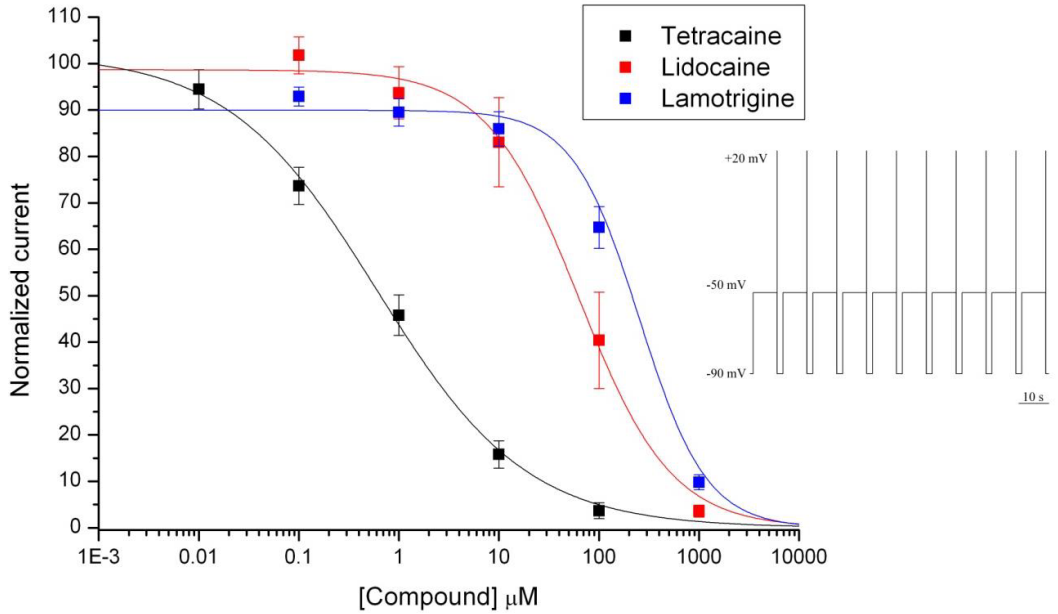

<u>$hNa_V1.8/\beta_1$ Pharmacology.</u> **Left:** Typical current traces showing the inhibition of hNav1.8 currents by increasing doses of lamotrigine. Control current before lamotrigine addition shown in black. **(Right).** Dose-response curves of tetracaine, lidocaine and lamotrigine on the hNav1.8/β1 current. Voltage protocol shown in inset (Manual Patch Clamp Data).

rNa$_V$1.8 in ND7-23 Cells (CYL3050)

BACK

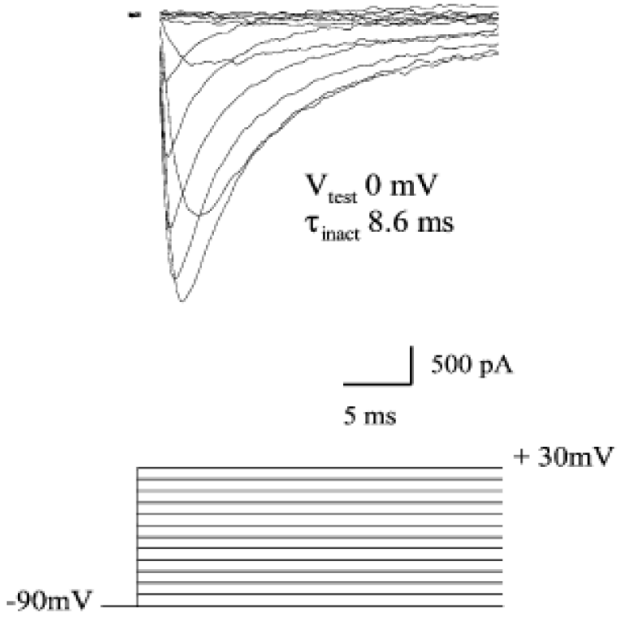

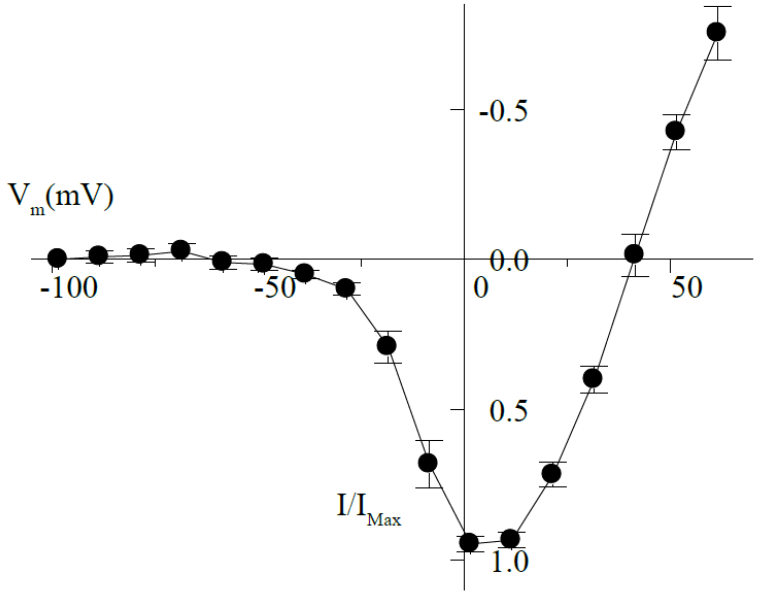

rNa$_V$1.8 Raw Data Currents and Current-Voltage Relationship. Typical current traces **(Left)** for rNa$_V$1.8 evoked by depolarizing voltage steps. **Right:** The peak current at each test potential was normalized to the maximum current (I/Imax) obtained from a given cell (Data are mean ± SEM, n=6). Currents measured in the presence of 100 nM TTX (Manual Patch Clamp Data).

rNa$_V$1.8 in ND7-23 Cells

BACK

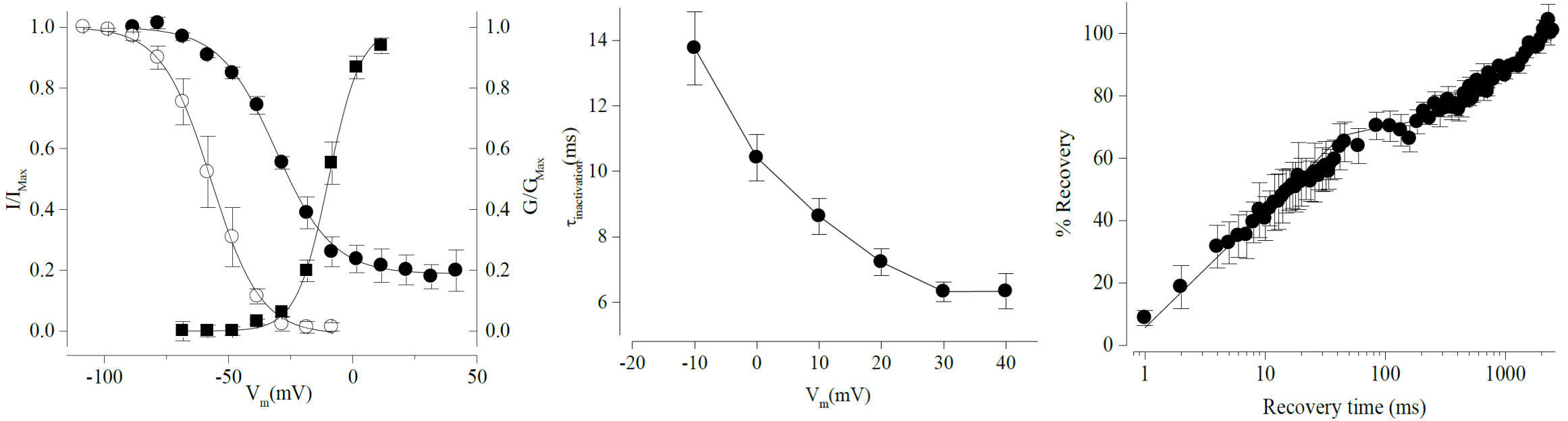

rNa$_V$1.8 Voltage Dependence of Activation and Inactivation. **Left:** Conductance-voltage (G/V) graph (■), and inactivation curves measured for pre-pulse durations of 4 s (○) and 15 ms. **Middle:** Voltage dependence of fast inactivation. The rates of inactivation (τ) at different potentials were determined by fitting the decay phase of the current trace to a single exponential function. **Right:** Currents were activated with twice (holding potential -90 mV, test potential 0 mV, 50 ms) with an incremental time delay between the two pulses (recovery time). The peak current evoked by the second pulse (I2) was normalized relative to the peak evoked by the first pulse (I1) and plotted against the logarithm of the recovery time. The line of best fit is a double exponential of the form y = A1*(1−exp(−t/τ1)) + A2*(1−exp(−t/τ2)) where t is the time, τ1 and τ2 are the two recovery time constants (13 and 2271 ms respectively) and A1 and A2 are the relative amplitudes of each exponential (45% and 59% respectively). In all panels, each point represents the mean ± SEM for at least 3 different cells obtained on at least 3 different experimental days. (Manual Patch Clamp Data).

rNa$_V$1.8 in ND7-23 Cells

BACK

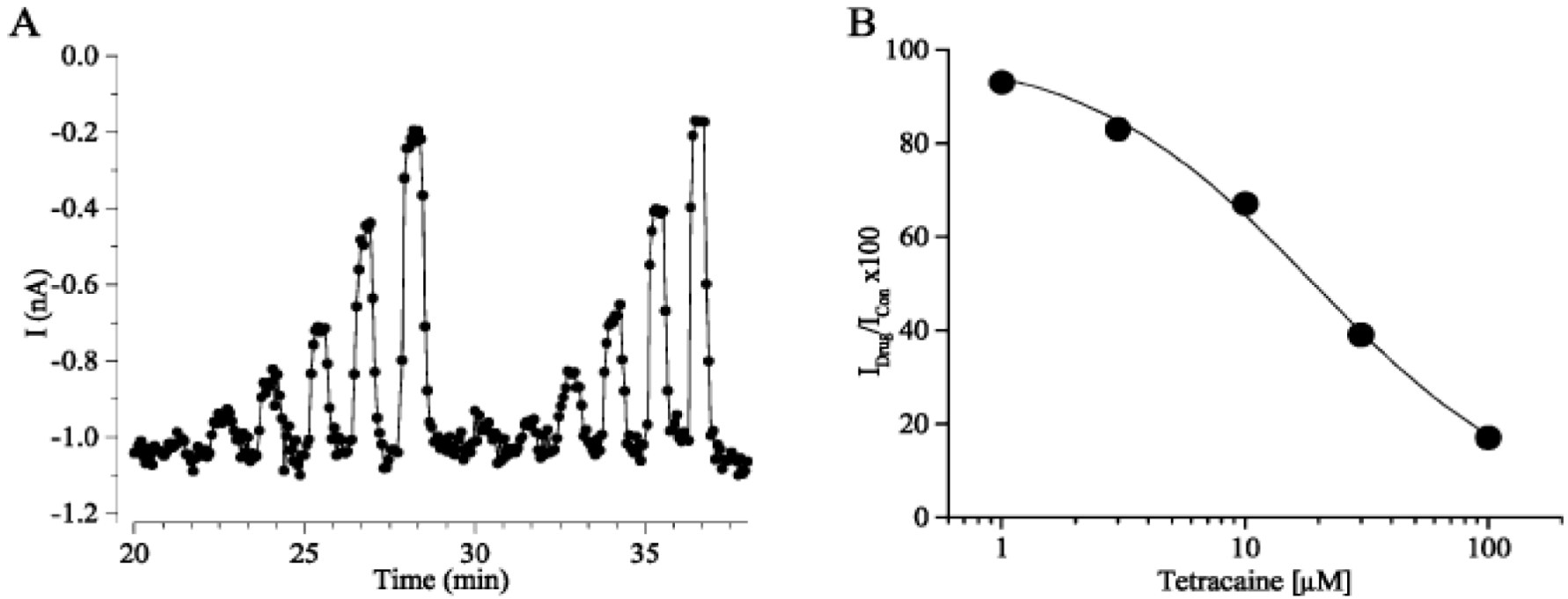

rNa$_V$1.8 Pharmacology. **Left:** Time course of currents evoked from test pulses (holding potential -90 mV, test potential 0 mV, 50 ms, every 4 s) following repeated addition of increasing concentrations of tetracaine (0.3–100 µM). **Right:** Mean concentration–response curve to tetracaine. The mean IC_{50} value was 12.5 µM and the slope 1.02.

rNa$_V$1.8 in ND7-23 Cells

BACK

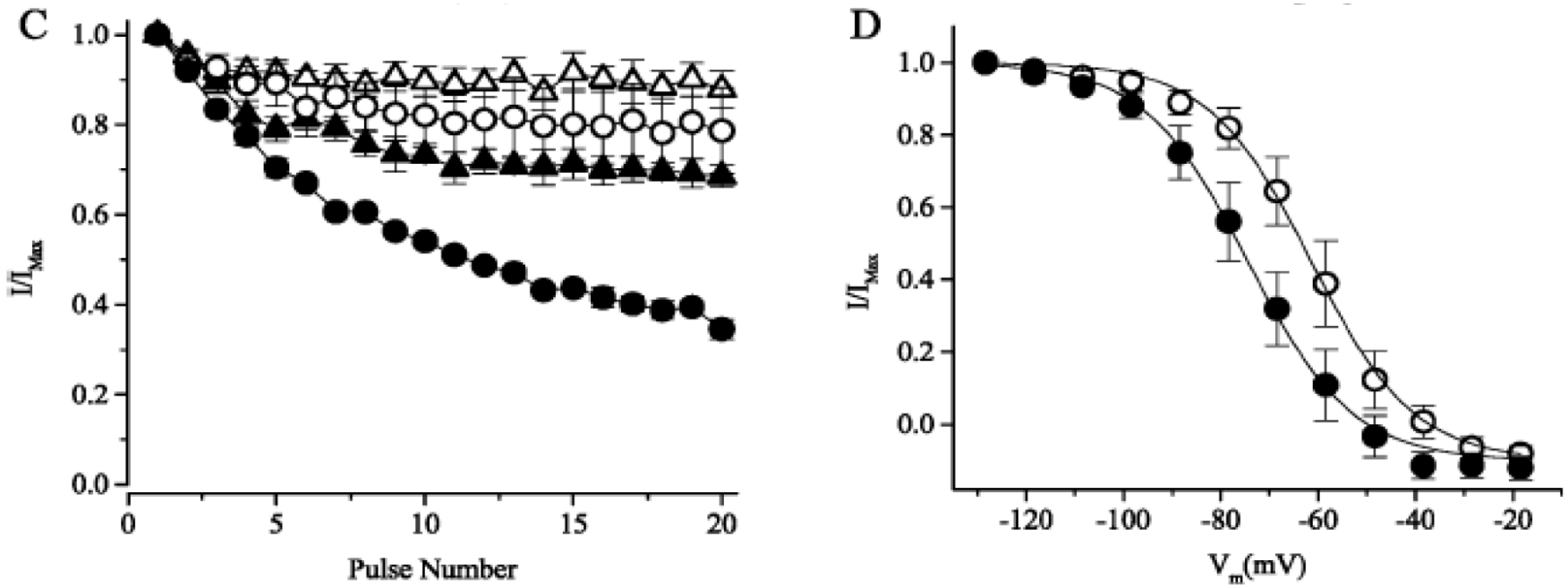

hNa$_V$1.8β$_1$ Pharmacology. **Left:** Frequency-dependent inhibition by tetracaine. Peak current amplitudes from 20 consecutive pulses (holding potential -90 mV, test potential 0 mV, 20 ms) in the absence (open symbols) and presence (solid symbols) of 3 μM tetracaine at frequencies of 2 Hz (▲/Δ) and 10 Hz (●/○). The current is normalized to the first pulse in each case, both in the absence and presence of drug, to account for the tonic (non-use-dependent) drug block. Note the greater blocking effect of tetracaine at higher stimulation frequencies. **(Right).** The steady state inactivation curve in the presence (●) and absence (○) of 10 μM tetracaine. (Manual Patch Clamp Data).

$rNa_V1.8$ in ND7-23 Cells

BACK

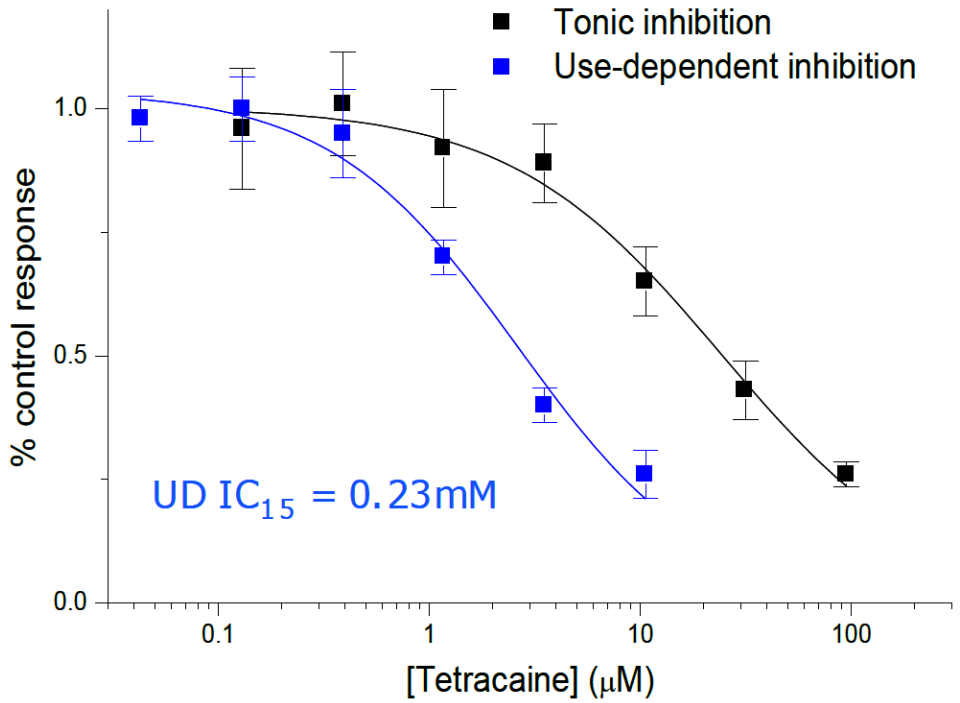

Use-Dependent Blockade of $rNa_V1.8$ Currents. Concentration response curves for tetracaine showing a use-dependent mechanism of action. 20 ms pulses were applied at 10 Hz, UD_{15} is the concentration giving use-dependent block of 15%. (IonWorks HT Data)

rNa$_V$1.8 in ND7-23 Cells

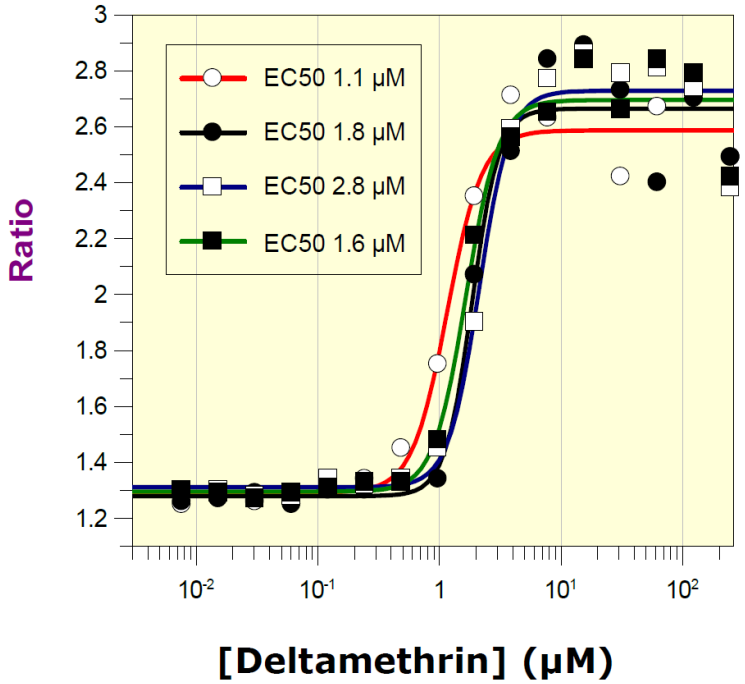

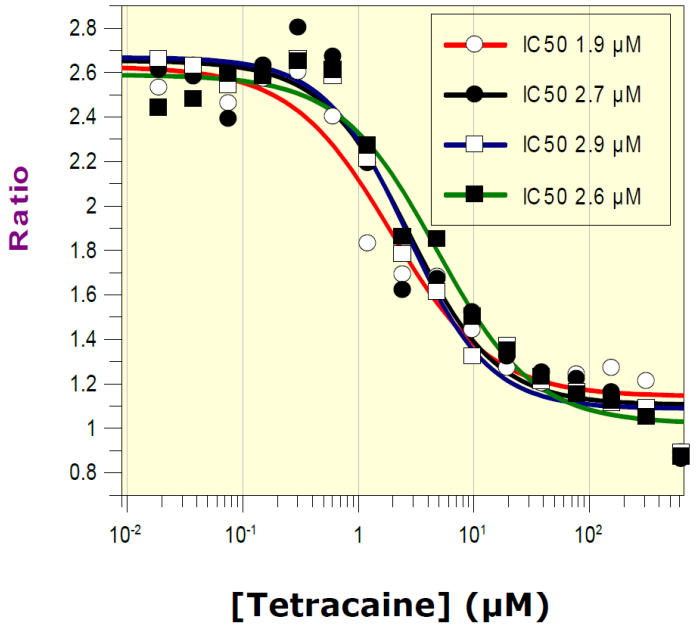

BACK

rNa$_V$1.8 Agonist and Antagonist Fluorescent Assay. In the presence of voltage sensitive probe fluorescent dyes (VSP) the sodium channel opener, deltamethrin, induced Na^+-dependent membrane potential depolarizations as indicated by an increase in the relative ratio of fluorescence of the two dyes. **Left:** Concentration response curves to deltamethrin. **(Right).** Concentration response curves for the inhibition of the deltamethrin-induced responses by the sodium channel inhibitor tetracaine (ImageTrak Data).